

APPENDIX A – ATTACHMENT A-2

**SEISMIC SOURCE CHARACTERISTICS OF
ONSHORE ROSE CANYON FAULT**

By

**Dr. Thomas Rockwell
San Diego State University**

INTRODUCTION

The following document has been prepared at the request of Southern California Edison (SCE) in consultation with technical members of their Seismic Hazard Assessment Program (SHAP).

The onshore traces of the Rose Canyon (RC) Fault Zone, as currently mapped through San Diego, are shown on Figure A2-1 (Rockwell, 2010a). The onshore evidence for the presence and recent activity of the Rose Canyon Fault Zone is abundant, with tectonic geomorphic expression of the active traces clearly evident in early aerial photography (Treiman, 1993; Lindvall and Rockwell, 1995, Rockwell, 2010a). As presented in Rockwell (2010a), 3-D trench data suggest that the most recent earthquake on the fault that resulted in surface rupture occurred sometime between AD 1523 and 1769. These 3-D trenching data further suggest that about 3 m of right-lateral, strike-slip surface displacement occurred during this event, with a 1:10 ratio of vertical to horizontal displacement.

Although the evidence for onshore rupture of the RC fault is not specific to the fault traces offshore of SONGS, these onshore data are some of the only available to address the size and frequency of earthquakes that may be expected from the Newport-Inglewood-Rose Canyon (NI/RC) Fault System, and therefore supports its seismic source characteristics. In particular, the onshore data supports the argument that the high-angle, right-lateral, strike-slip NI/RC Fault System is a primary seismic source fault whereas the nearby, shallow-dipping normal, oblique, and reverse faults are subsidiary.

The following sections of this appendix provide more information regarding:

1. How the onshore RC data supports the conclusion that the high-angle, right-lateral, strike-slip NI/RC Fault System is the primary seismic source fault, as was concluded during the 1980s licensing of the plant, and as was recently incorporated into the preparation of the current version of the National Seismic Hazard Map (USGS, 2009);
2. Why these data are appropriate to use to define the current model of the NI/RC Fault System for incorporation into the update of the plant's Probabilistic Seismic Hazard Assessment, and the update of its deterministic tsunami assessment with a Probabilistic Tsunami Hazard Assessment; and
3. The identification of recommended future research that will further strengthen our understanding of the potential hazards associated with the NI/RC Fault System.

PRESENCE AND LEVEL OF ACTIVITY

The active surface trace of the RC fault can clearly be mapped southward from the La Jolla coastline, up over Mount Soledad, down through Rose Canyon, across the San Diego River Valley, through Old Town San Diego and downtown San Diego, and across Coronado Island based on analysis of early aerial

photography (Treiman, 1993, Lindvall and Rockwell, 1995, Rockwell, 2010a). The location of the fault is marked by the presence of scarps, deflected drainages, a sag and several pressure ridges, all of which attest to its recent activity (Figure A2-2). Most of these features also demonstrate that the fault has been repeatedly active throughout the late Quaternary with essentially the same kinematic motion. The traces beneath San Diego Bay have been imaged by shallow seismic techniques, where several strands of the fault clearly cut Holocene marine sediments (Kennedy and Clarke, 1996), also indicating that the Rose Canyon fault is young and active. Surprisingly, an early (Glover, 1876) artists rendition of Newtown (present day downtown San Diego) shows the trace of the fault as a scarp and several deflected drainages precisely where recent trenching has determined to be the main traces of the fault (see Figure A2-3), and supports the recency of displacement that has been demonstrated in the trenching studies (Lindvall and Rockwell, 1995; Rockwell, 2010a).

The linearity of the fault trace across hilly topography argues that the fault maintains a steep dip through much of San Diego, except in the Mount Soledad area, where the fault appears to dip to the southwest beneath the uplift. The fault strike in this area is also more westerly, consistent with a restraining bend geometry that has resulted in the uplift of the mount. Marine terraces on the southwest flank of the uplift (Kern, 1977; Kern and Rockwell, 1992), along with the presence of the Linda Vista Formation marine terrace alluvium capping Mount Soledad, attest to the higher rate of uplift of the restraining bend area (0.25 mm/yr) relative to the surrounding coastal plain (0.13 mm/yr) (Kern and Rockwell, 1992), with the background regional uplift attributed to rift-flank uplift from extension in the Gulf (Mueller et al., 2009).

The level of late Quaternary fault activity is indicated by both the relatively large lateral deflections of stream channels that are incised into low marine terraces (Figure A2-4), and by the results of the three-dimensional trenching. These observations suggest a lateral slip rate of about 2 mm/yr during the late Quaternary (Rockwell, 2010a).

SEISMIC CHARACTERISTICS

The expected length of a future rupture on the Rose Canyon fault may be limited by structural controls, such as steps, bends, and changes in strike that may be large enough to terminate dynamic rupture. For the southern termination, the right-step between the Rose Canyon and Descanso faults forms the depression occupied by San Diego Bay (Figure A2-1), and is likely large enough to arrest dynamic slip. This step exceeds 5 km in step-over width (Figure A2-5), which is more than the largest releasing step that has been ruptured through in historical, well-documented strike-slip earthquakes (Wesnousky, 2008). Based on this, the southern termination of future large earthquakes on the Rose Canyon fault is expected to be in San Diego Bay.

For the northern termination, there are several structural features that may play a role, but none are as large as the step across San Diego Bay. The left bend in the Rose Canyon fault that facilitated the uplift of Mt. Soledad is only on the order of a couple kilometers in cross-fault dimension (Figure A2-5) and many historical earthquakes have ruptured through bends and steps of such dimensions (Wesnousky, 2008) (cf. the 1968 Mw6.4 Borrego Mountain earthquake ruptured across the 1.5-2 km wide Ocotillo Badlands with less than a half meter of displacement, Clark, 1972). Thus, the Mt. Soledad bend and uplift is not likely to be large enough to define a rupture segment boundary, especially if the Rose Canyon fault has 3 m of displacement in Rose Creek. Furthermore, it is a continuous surface fault

through the region of this bend based on the geomorphology and extensive local trenching (Lindvall and Rockwell, 1995; Rockwell and Murbach, 1999).

Farther north, the Rose Canyon fault steps to the right (releasing step) near Oceanside, but the dimensions of the step are only on the order of 2-3 km or so (Figure A2-5). This can be a significant barrier to rupture in moderate earthquakes, but is less likely to stop a large dynamic displacement. More significantly, however, the Rose Canyon fault has a more westerly strike to the northwest of this step, and the change in azimuth is on the order of 15 degrees from the average strike of the fault between Oceanside and San Diego Bay. The combination of the releasing step plus a change in fault strike make the Oceanside step a likely termination zone for ruptures, although a through-going rupture cannot be precluded.

The SONGS sits along the coast between Oceanside and the San Joaquin Hills uplift, and there are no major, obvious structural complexities that can be used to segment the Rose Canyon fault along this stretch. However, the San Joaquin Hills may represent uplift associated with a step from the northern termination of the Rose Canyon to the Newport- Inglewood fault zone. Grant et al. (2002) consider the uplift as the consequence of slip on a blind thrust, but likely structurally linked to the Newport- Inglewood fault zone (Grant et al., 1999, 2000). A closely related model is that the Rose Canyon fault bends northward and steps left across the hills to the Newport Inglewood fault, producing uplift by slip on the low-angle accommodation fault. An alternative model is that the San Joaquin uplift is related to a blind thrust system, the Oceanside thrust, that accommodates shortening in the Borderland (Rivero et al., 2000). In any case, the San Joaquin uplift is a structural complexity and may serve to segment the offshore zone of faulting.

An approach to shedding light on this problem, and to better constrain the likely sizes and termination zones for future earthquakes associated with the Rose Canyon and Newport-Inglewood faults, is to assess the current paleoseismic data in terms of whether they support co-seismic rupture of these faults together in the past. Grant and Rockwell (2002) documented the occurrence of a sequence of large earthquakes that ruptured the coastal zone of faults in the past few hundred years, but was pre-historical in age. This sequence involved the onshore Agua Blanca fault in northern Baja California, as well as the onshore Rose Canyon fault in San Diego and the San Joaquin Hills fault beneath Newport Bay, and was succeeded by the 1933 rupture of the Newport- Inglewood fault in Los Angeles Basin (Figure A2-6). Based on radiocarbon dating of the most recent earthquakes on these three faults, this sequence appears to have propagated northward, because rupture of the Agua Blanca fault is apparently the oldest of the events. In actuality, the dates of these three events all overlap to some degree, but there is the appearance that events to the north are younger than those to the south. Furthermore, it is unlikely that an earthquake ruptured both the Agua Blanca- Descanso and Rose Canyon faults simultaneously because of the large step-over at San Diego Bay. Combined with the occurrence of the 1933 event, which is clearly the youngest, the interpretation presented by Grant and Rockwell (2002) seems reasonable. Alternatively, as the most recent event on the Rose Canyon fault overlaps with the interpreted uplift of Newport Bay, it is possible that the entire Rose Canyon fault ruptured in a large earthquake just prior to the Mission period, and that the Newport Bay uplift is a consequence of this event. Because of the inherent problems in precise radiocarbon dating in this time period, this question may be difficult to resolve. Nevertheless, the occurrence of the sequence (or single event) supports the idea that the San Joaquin uplift is structurally tied to the coastal system of strike-slip faults.

There is a clearer difference in timing between Rose Canyon and onshore Newport- Inglewood fault ruptures (Figure A2-6; compiled from Grant et al., 1997; Grant and Rockwell, 2002; Leon, et al., 2009), which argues against the likelihood of a very long rupture. Although the timing is similar, Grant and Rockwell argue that the pre-Mission sequence of ruptures represent multiple events, and likely propagated northward, culminating in the relative small M6.4 1933 Long Beach earthquake. It is noteworthy that the 1933 earthquake is not known to have ruptured the surface, and there were plenty of people around who should have noticed a significant rupture. Grant et al. (1997) use this observation to argue that the Holocene events identified for the Newport-Inglewood fault at Bolsa Chica likely represent larger earthquakes than that which occurred in 1933.

The pre-historic Newport-Inglewood and Compton-Los Alamitos events are nearly indistinguishable in timing (Figure A2-6), considering their large uncertainties. Nevertheless, they both have a similar return period for large earthquakes – those that can be identified by CPT and core correlation techniques, which implies that they are larger than 1933. One could argue that the Compton Los Alamitos and Newport- Inglewood faults ruptured together in the largest earthquakes, suggesting that they are kinematically linked. This may support Wright's (1991) interpretation of the Compton fault as a high angle oblique splay of the Newport-Inglewood fault. In any case, it is clear that the 1933 earthquake is smaller, and it was not associated with a large event on the Compton structure. Barrows (1974) does, however, document that the area between the Los Alamitos and Newport-Inglewood faults was uplifted in the 1933 earthquake (Figure A2-7), again indicating a structural tie between these structures.

Rose Canyon fault has a very different paleoseismic record of past earthquakes than those faults to the north. The Rose Canyon fault experienced a cluster of events in the early Holocene, followed by a hiatus of several thousand years (Figures A2-6)(Rockwell, 2010a). Although one could argue that the mid-Holocene event documented at Bolsa Chica on the Newport-Inglewood fault could correlate to one of the mid-Holocene Rose Canyon events, it is clear that the others do not, as there are no other recognized events during this cluster at Bolsa Chica. Unfortunately, the San Joaquin Hills record is too short (one event) to assess whether there is a correlation between Rose Canyon events and uplift at Newport Bay. Nevertheless, it appears that the Rose Canyon earthquake history is generally dissimilar to that of the Newport-Inglewood fault, which likely means that these faults do not typically rupture together.

In summary, the Rose Canyon fault is interpreted as a distinct seismic source that does not likely rupture with the Newport-Inglewood fault to the north, nor the Agua Blanca-Descanso fault to the south. If the Oceanside step-over is a barrier to rupture propagation, it would divide the Rose Canyon fault into two roughly similar-length sections: a 65 km segment from San Diego Bay to Oceanside, and a 55 km segment from Oceanside to the San Joaquin Hills. From the short paleoseismic record at Newport Bay, it is not possible to test long-term patterns of recurrence between these two segments. Further, due to the overlap in ages between the most recent ruptures inferred for these two segments (assuming the Newport Bay uplift is associated with a northern Rose Canyon rupture that involved the San Joaquin Hills), one cannot preclude rupture of the entire Rose Canyon fault for a distance of more than 100 km. However, I consider this model a lower likelihood than rupture of individual segments and weight it at 25%, versus 75% for the more segmented rupture behavior.

For PSHA and PTHA seismic source characterization model, I suggest using the maximum slip rate range of 1.1 to 2.5 mm/yr, with the best estimate of 1.5-2.5 mm/yr, with the following weights:

0.5 (0% weight)

- 1.0 (10% weight)
- 1.5 (30% weight)
- 2.0 (40% weight)
- 2.5 (20% weight)
- 3.0 (0% weight)

For calculations that involve lapse time since the most recent event (time-based probabilities), you may want to consider that the Rose Canyon fault apparently behaves in a clustered mode, where the time between events within a cluster is shorter than the average long-term recurrence interval. This can be viewed, in effect, as variations in short term slip rate, with the period between about 10-5 ka having a higher rate than the long term average (Figure A2-8), the rate from 5-0.5 ka being essentially zero, and the current rate somewhat uncertain. Considering that the fault experienced a recent large earthquake after several thousand years of quiescence, and if it is reasonable to assume that we have entered another cluster which reflects a short-term increase in slip rate, then it follows that the time to the next event will be shorter than that inferred from the long-term average. Rockwell (2010a) inferred the intra-cluster recurrence interval to be less than 1 ka, with five events between 9.3 and 5 ka. This yields a recurrence interval of about 900 years within that cluster. If each event was as large as the most recent event, about 3 m, this would suggest a slip rate of more than 3 mm/yr for this interval. Considering that short and long-term fault behavior of faults is somewhat enigmatic and a current topic of debate within the scientific community (see Rockwell, 2010b), I would suggest using the long-term rate with an 80% weight, and consider using an alternative weighting scheme for slip rate (in mm/yr) with a 20% overall weight as follows:

- 0.5 (0% weight)
- 1.0 (10% weight)
- 1.5 (30% weight)
- 2.0 (30% weight)
- 2.5 (20% weight)
- 3.0 (10% weight)

KEY REMAINING UNCERTAINTIES

There are two key uncertainties that need to be resolved. For understanding the short and long-term pattern of earthquakes on the Rose Canyon fault, and their implications for future activity, it is critical to test the cluster model of Rockwell (2010a) by resolving whether there were any surface ruptures between about 5 and 0.5 ka. There was no deposition at the Rose Creek site during this period, and the inference of no ruptures is based on the strength of a soil that is developed across the earlier Holocene fault strands (Rockwell, 2010a), so it is possible that an event was missed or not well-recorded. Paleoseismic investigations in mid-late Holocene sediments across the Rose Canyon fault could resolve

whether other events may have occurred, as well as potentially determine their amount of displacement. This may affect our perception of recurrence and earthquake magnitude along the Rose Canyon Fault.

The other remaining major question relates to the nature of the inferred shortening deformation suggested by Rivero et al. (2000) in the offshore region, and its relationship to the Rose Canyon fault. Geodetic observations clearly see significant right-lateral shear between San Clemente Island and Monument Peak, but there is no observable shortening or extension (figure A2-9). In fact, the right-lateral nature of the Agua Blanca fault in Baja California, along with its westerly strike, could be interpreted that there should be a small amount of continuing extension in the Borderland region (Wetmore et al., 2010 in review). Therefore, the cause of the apparent folding in the offshore Inner Borderland Region (Rivero et al., 2000) remains open to interpretation.

There are other areas where similar patterns of deformation have been observed, and it may prove valuable to assess these areas in terms of their overall structural style and seismic potential. One area that appears to have slip partitioned between strike-slip and convergence is in central California. In this area, the San Andreas fault (at 35 mm/yr) is the undisputed dominant seismic source, both in terms of magnitude and frequency. Nevertheless, a small component of shortening, estimated at no more than 3 mm/yr from geodetic data, is partly expressed as a series of folds and blind thrust faults to the east of the San Andreas fault (Coalinga anticline, Kettleman Hills, etc.: Yerkes, 1990, Wentworth, 1990). In this case, these secondary seismic sources are clearly seismically active, having produced several earthquakes in the M5.5- M6.5 range during the instrumental period, but are subordinate to the San Andreas fault. However, in comparison to the Inner Borderland, the central California example is clearly different because 1) there are clearly-defined folds that overlie blind thrusts; 2) these folds have significant structural relief and fold Holocene terraces; 3) there is a clear geodetic signal to the shortening; 4) there are earthquakes with thrust mechanisms clearly associated with these structures.

In the Inner Borderland Region, the association is not nearly as clear. There is a Miocene detachment surface, above which there has apparently been some folding (Rivero et al., 2000). However, there is no recognizable geodetic signal of shortening, nor is the seismicity clearly associated with this inferred detachment surface. An analogous situation is present in the western Salton Trough along the southern San Jacinto fault zone.

The West Salton Detachment-San Jacinto Example: The West Salton Detachment underlies much of the western Salton Trough east of the Peninsular Ranges from Borrego Valley and to the south to the Mexican Border (Axen and Fletcher, 1998). In this area, the high-angle, right-lateral San Jacinto fault cuts and offsets the West Salton Detachment and is clearly the dominant structure. Of note is the ubiquitous presence of extensive folding in the Borrego Badlands, San Felipe Hills, and Fish Creek Badlands, all of it post-detachment in age and all of it related to the continuing development of the southern San Jacinto fault zone (Dorsey and Janecke, 2002; Lutz et al., 2006).

There are many similarities between the western Salton Trough and the Inner Borderland Region. First, there is young folding above the Miocene-Pliocene detachment system, with the folding in the western Salton Trough being of substantially greater magnitude and significance than the folding in the offshore region. Furthermore, the folding is not only associated with bends in the strike-slip faults, but rather, appears to be more regionally scaled and related to secondary space accommodation above the detachment surface driven by the dominant strike-slip faulting. Second, neither region shows a geodetic signal of convergence, but rather, GPS and InSAR show virtually pure strike slip at the regional scale for

the southern San Jacinto fault zone (see Fialko, 2006). Third, at least one fold grew during the 1987 Superstition Hills earthquake sequence in the western Salton Trough (Klinger and Rockwell, 1989), so there is a demonstrable association between strike-slip faulting and fold growth in this area. These and other similarities warrant a thorough examination and comparison between these two structural domains, in part because the western Salton Trough is well-studied and easily accessible.

RECOMMENDATIONS TOWARD RESOLVING REMAINING UNCERTAINTIES

For the Rose Canyon Fault itself, there are potential paleoseismic study sites to resolve whether the fault sustained displacement between about 5 and 0.5 ka. The sediments within and adjacent to the San Diego River are of the appropriate age, as river aggradation probably ceased about the time sea level rose to its present level at about 5-6 ka, and after that, sedimentation on the flood plain has locally preserved alluvium of various ages in the 0.5 to 5 ka timeframe. One area that may preserve such a record is in Old Town, where the landscape is only minimally altered. One potential site is in a golf course that essentially preserved the original topography; the fault is still expressed as a linear depression. The golf course property is owned by the City of San Diego, although it is currently under lease. Another potential site is close to the Lindvall and Rockwell (1995) trench site where a closed depression (sag) is observed in the 1928 and 1941 aerial photography. This is on private land, so access will likely be an issue. A third general site is in the flood plain of the San Diego River in Mission Valley. The fault is expressed in the 1928 aerial photographs, so the fault location can be determined with some work. The fault location may be better determined with CPT or geophysical means, once it is approximately located by interpretation of the old aerial photography. It may be possible to trench along a street, once the fault is well located.

To assess and understand the significance of the folding above the detachment surface in the offshore region, I also recommend that we thoroughly document the structural styles, rates of folding and faulting, etc. for the analogous Western Salton Trough and compare to that of those observed for the Inner Borderland Region. We need to better understand the relationship between the strike-slip faulting and the folding in the Borderland, and the western Salton Trough is far more open to study and analysis because it is sub-aerial and easily accessible. In the southern San Jacinto fault zone, we can better understand how, and when, the folding occurred, and how it relates to the dominant strike-slip faulting, perhaps even to individual events. We should also reanalyze the geodetic signals of these two areas for a component of convergence and test whether a small shortening component can be precluded or accepted.

REFERENCES

- Axen, G. J., and Fletcher, J. M. 1998. Late Miocene-Pleistocene extensional faulting, northern Gulf of California, Mexico and Salton Trough, California. *Int. Geol. Rev.* 40:217–244.
- Barrows, A.G., 1974, A review of the geology and earthquake history of the Newport- Inglewood structural zone, southern California: California Division of Mines and Geology Special Report 114, 115 p.
- Clark, M.M., 1972, Surface Rupture Along the Coyote Creek Fault, USGS Professional Papers, 787, 55-86.
- Dorsey, R. J., and Janecke, S. U. 2002. Late Miocene to Pleistocene West Salton detachment fault and basin evolution, southern California: new insights. *Geol. Soc. Am. Abstr. Program* 34:248.
- Fialko, Y., 2006, Interseismic strain accumulation and the earthquake potential on the southern San Andreas fault system, *Nature* v. 441, 968- 971.10.1038/nature04797.
- Glover, E.S., 1876, Bird's Eye View of San Diego, California. Map published by Schneider and Kueppers, San Diego.
- Grant, L.B., Waggoner, J.T., Rockwell, T.K., and von Stein, C., 1997, Paleoseismicity of the north branch of the Newport-Inglewood fault in Huntington Beach, California: *Bulletin of the Seismological Society of America*, v. 87, pp. 277-293.
- Grant, L. B., K. J. Mueller, E. M. Gath, H. Cheng, R. L. Edwards, R. Munro and G. L. Kennedy, Late Quaternary Uplift and Earthquake Potential of the San Joaquin Hills, southern Los Angeles Basin, California, *Geology*, v. 27, no. 11, p. 1031-1034, 1999.
- Grant, L. B. L. J. Ballenger, and E. E. Runnerstrom. Coastal uplift of the San Joaquin Hills, Southern Los Angeles basin, California, by a large earthquake since 1635 A.D. *Bulletin Seismological Society of America*, v. 92, no. 2, p.590-599, 2002.
- Grant L. B. and Rockwell, T. K., 2002, A northward propagating earthquake sequence in coastal southern California?: *Seismological Research Letters*, v. 73, no. 4, p. 461-469.
- Kennedy, M. P. and Clarke, S.H., 1996, Analysis of late Quaternary faulting in San Diego Bay and hazard to the Coronado Bridge, prepared for Caltrans.
- Kern, J.P., 1977, Origin and history of upper Pleistocene marine terraces, San Diego, California, *Geological Society of America Bulletin*, v. 88, p. 1553-1566.
- Kern, J.P. and Rockwell, T.K., 1992, Chronology and deformation of Quaternary marine shorelines, San Diego County, California: in *Quaternary Coasts of the United States: Marine and Lacustrine Systems: Society of Economic Paleontologists and Mineralogists Special Publication.No. 48*, p. 377-382.
- Klinger, R.E. and Rockwell, T.K., 1989, Flexural-slip folding along the eastern Elmore Ranch fault in the Superstition Hills earthquake sequence of November 1987: *Bulletin of the Seismological Society of America*, v. 79, no. 2, p. 297-303.

**SAN ONOFRE NUCLEAR GENERATING STATION
SEISMIC HAZARD ASSESSMENT PROGRAM
2010 PROBABILISTIC SEISMIC HAZARD ANALYSIS REPORT**

Leon, L.A., Dolan, J.F., Shaw, J.H., and Pratt, T.L., 2009, Evidence for large Holocene earthquakes on the Compton-Los Alamitos fault, Los Angeles, California. *Journal of Geophysical Research*, v. 114, B12305, doi:10.1029/2008JB006129.

Lindvall, S. and Rockwell, T.K., 1995, Holocene activity of the Rose Canyon fault, San Diego, California: *Journal of Geophysical Research*, v. 100, no. B12, p. 24121- 24132.

Lutz, A. T.; Dorsey, R. J.; Housen, B. A.; and Janecke, S.U. 2006. Stratigraphic record of Pleistocene faulting and basin evolution in the Borrego Badlands, San Jacinto fault zone, southern California. *Geol. Soc. Am. Bull.* 118:1377–1397.

Mueller, K., Kier, G., Rockwell, T. and Jones, C. 2009, Quaternary Rift-Flank Uplift of the Peninsular Ranges in Baja and Southern California by Removal of Mantle Lithosphere. *Tectonics*, v. 28, 17 p. doi:10.1029/2007TC002227.

Rivero, C., Shaw, J.H., and Mueller, K.J., 2000, Oceanside and Thirty Mile Bank blind thrusts: Implications for earthquake hazards in coastal southern California. *Geology*, v 28, p. 891-894.

Rockwell, T., 2010a, The Rose Canyon Fault Zone in San Diego; Proceeding of Fifth International Conference on Recent Advances in Geotechnical Earthquake Engineering and Soil Dynamics and Symposium in Honor of Professor I.M. Idriss; Paper No. EQ 5, 9pgs.

Rockwell, T., 2010b, The non-regularity of earthquake recurrence in California: Lessons from long paleoseismic records from the San Andreas and San Jacinto faults in southern California, and the north Anatolian fault in turkey, Proceeding of Fifth International Conference on Recent Advances in Geotechnical Earthquake Engineering and Soil Dynamics and Symposium in Honor of Professor I.M. Idriss; Paper No. EQ 5, 9pgs.

Rockwell, T.K. and Murbach, M., 1999, Holocene earthquake history of the Rose Canyon fault zone. USGS Final Technical Report for Grant No. 1434-95-G-2613, 36 p + App.

Treiman, J., 1993, The Rose Canyon fault zone, southern California, California Div. of Mines and Geology, Open File Report 93-02, 45 p.

USGS, 2009, Personal Communication.

Wentworth, C.M., 1990, Structure of the Coalinga region and thrust origin of the earthquake, in The Coalinga, California earthquake of May 2, 1983. U.S. Geological Survey Professional Paper 1487, p. 41-68.

Wetmore et al., 2010 in review, The Agua Blanca Fault in Baja California, submitted to *Tectonics*.

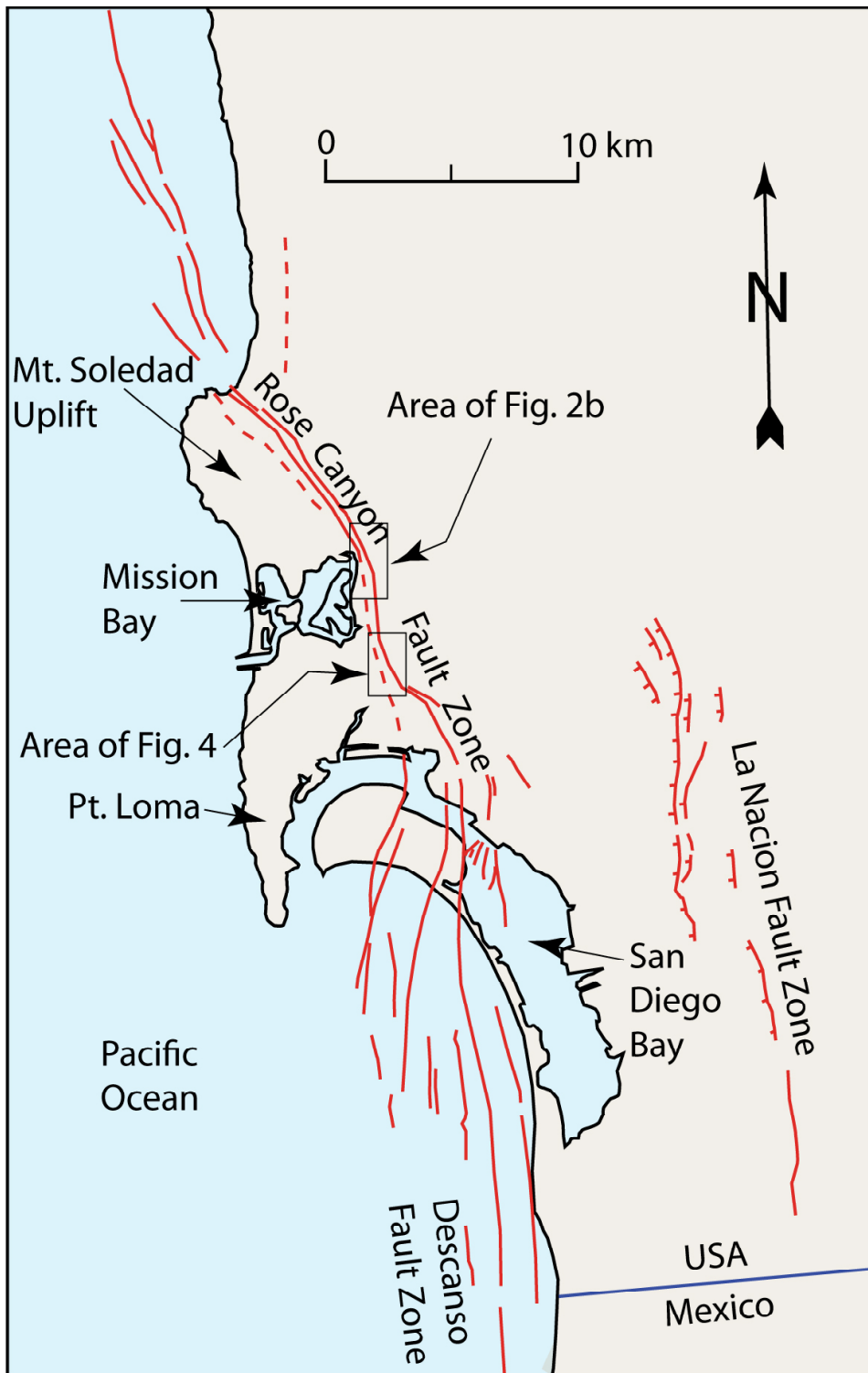
Wesnousky, S.G., 2008, Displacement and geometrical characteristics of earthquake surface ruptures: Issues and implications for seismic-hazard analysis and the process of earthquake rupture. *Bull. Seismological Society of America*, v. 98, p. 1609-1632.

Wright, T.L., 1991, Structural geology and tectonic evolution of the Los Angeles basin, California. In *Am. Assoc. Petroleum Geologists Memoir* 52, p. 35-134.

**SAN ONOFRE NUCLEAR GENERATING STATION
SEISMIC HAZARD ASSESSMENT PROGRAM
2010 PROBABILISTIC SEISMIC HAZARD ANALYSIS REPORT**

Yerkes, R.F., 1990, Tectonic setting, in The Coalinga, California earthquake of May 2, 1983. U.S. Geological Survey Professional Paper 1487, p. 13-22.





MAP OF THE MAIN ELEMENTS OF
THE ROSE CANYON FAULT IN SAN DIEGO

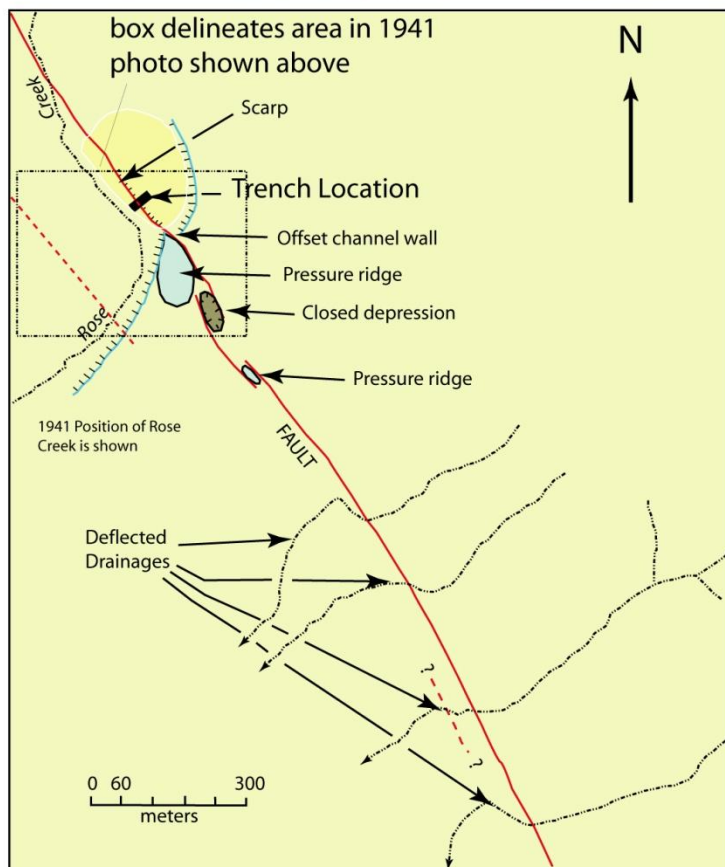
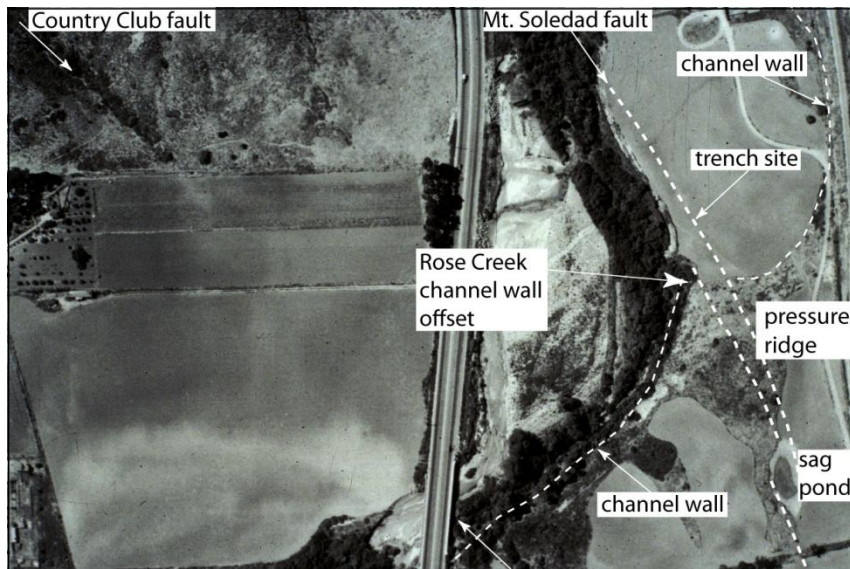
FIGURE
A2-1

SAN ONOFRE NUCLEAR GENERATING STATION
SEISMIC HAZARD ASSESSMENT PROGRAM



GeoPentech
Geotechnical & Geoscience Consultants

By Rockwell (2010)



NOTE: Annotated air photo (upper) shows detail of area in the box in the lower diagram (from Lindvall and Rockwell, 1995, Rockwell, 2010).



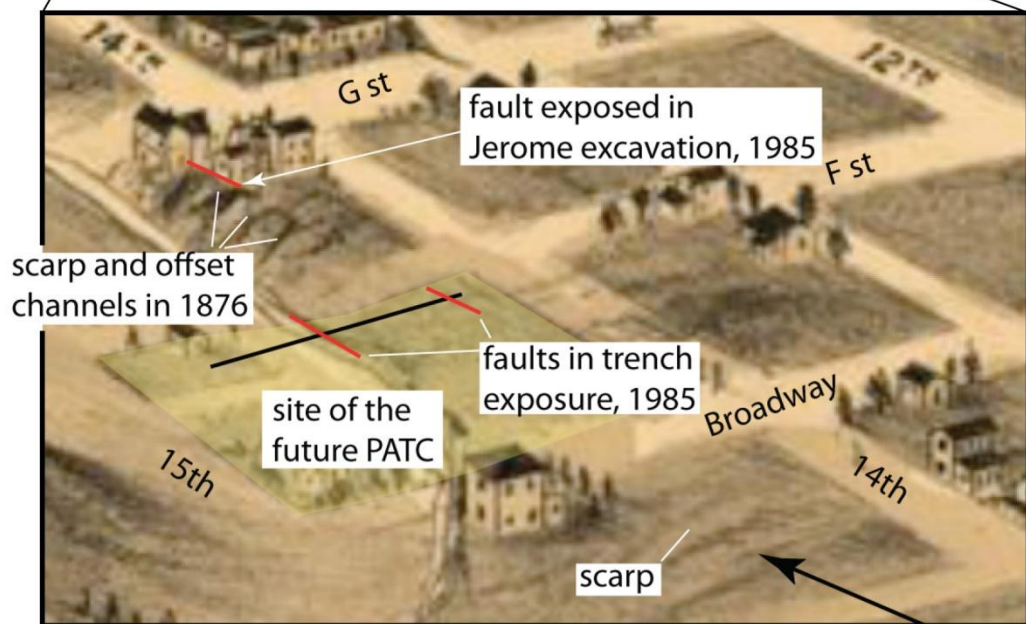
GeoPentech
Geotechnical & Geoscience Consultants

By Rockwell (2010)

INTERPRETIVE MAP OF TECTONIC GEOMORPHIC FEATURES IN THE ROSE CREEK AREA

FIGURE
A2-2

SAN ONOFRE NUCLEAR GENERATING STATION SEISMIC HAZARD ASSESSMENT PROGRAM



NOTE: Remarkably, the artist's eye picked out and drew scarps and deflected drainages along the Rose Canyon fault: the location of the fault in this area was determined by excavations in 1985 for the new Police headquarters building (PATC) and for a foundation excavation for a Jerome's warehouse.



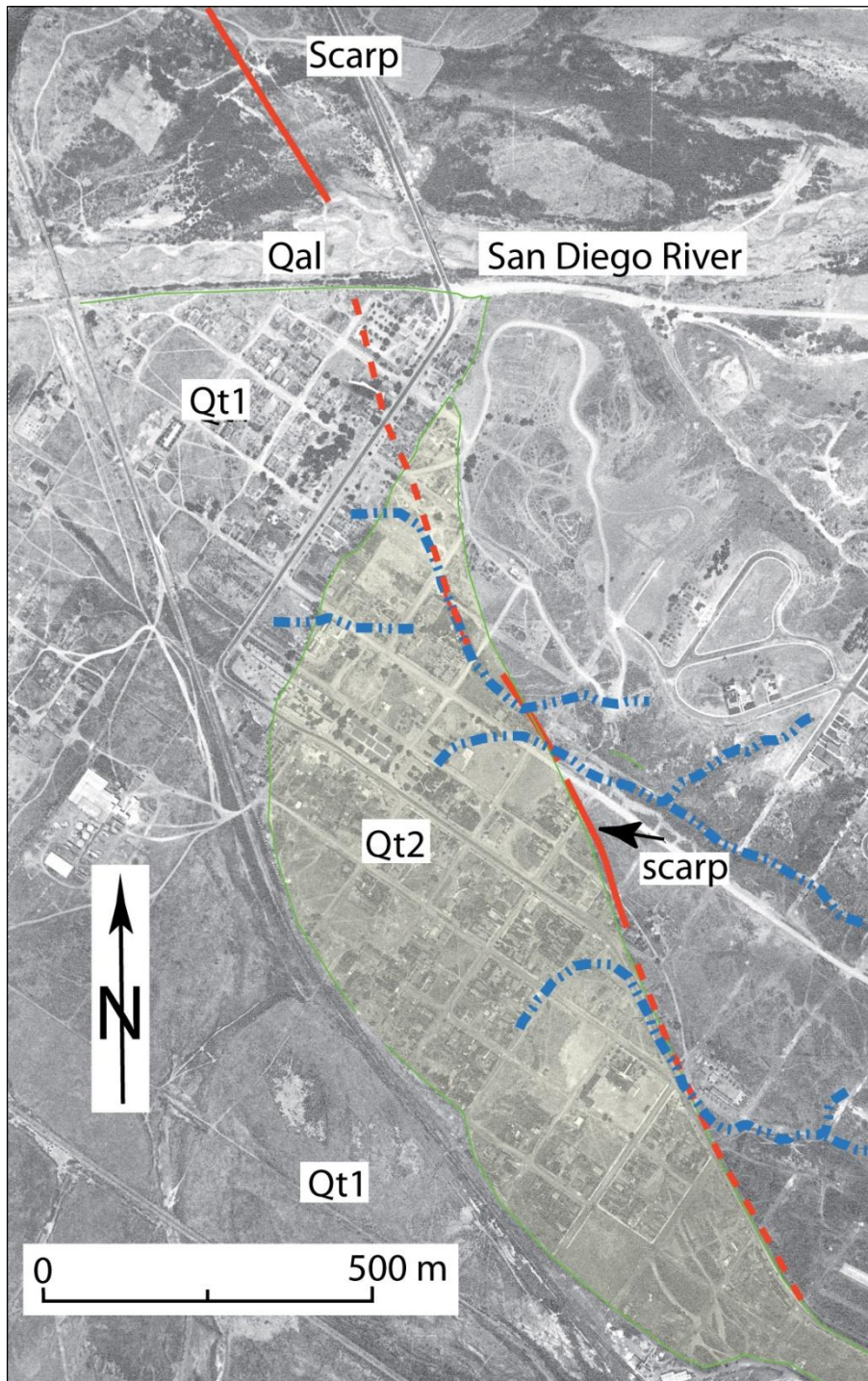
GeoPentech
Geotechnical & Geoscience Consultants

By Rockwell (2010)

**ANNOTATED ARTIST'S RENDITION
OF DOWNTOWN SAN DIEGO IN 1876**

**FIGURE
A2-3**

SAN ONOFRE NUCLEAR GENERATING STATION
SEISMIC HAZARD ASSESSMENT PROGRAM



NOTE: Note the deflected channels incised into the Qt2 surface, which is interpreted to be last the interglacial terrace based on its elevation (from Rockwell, 2010).



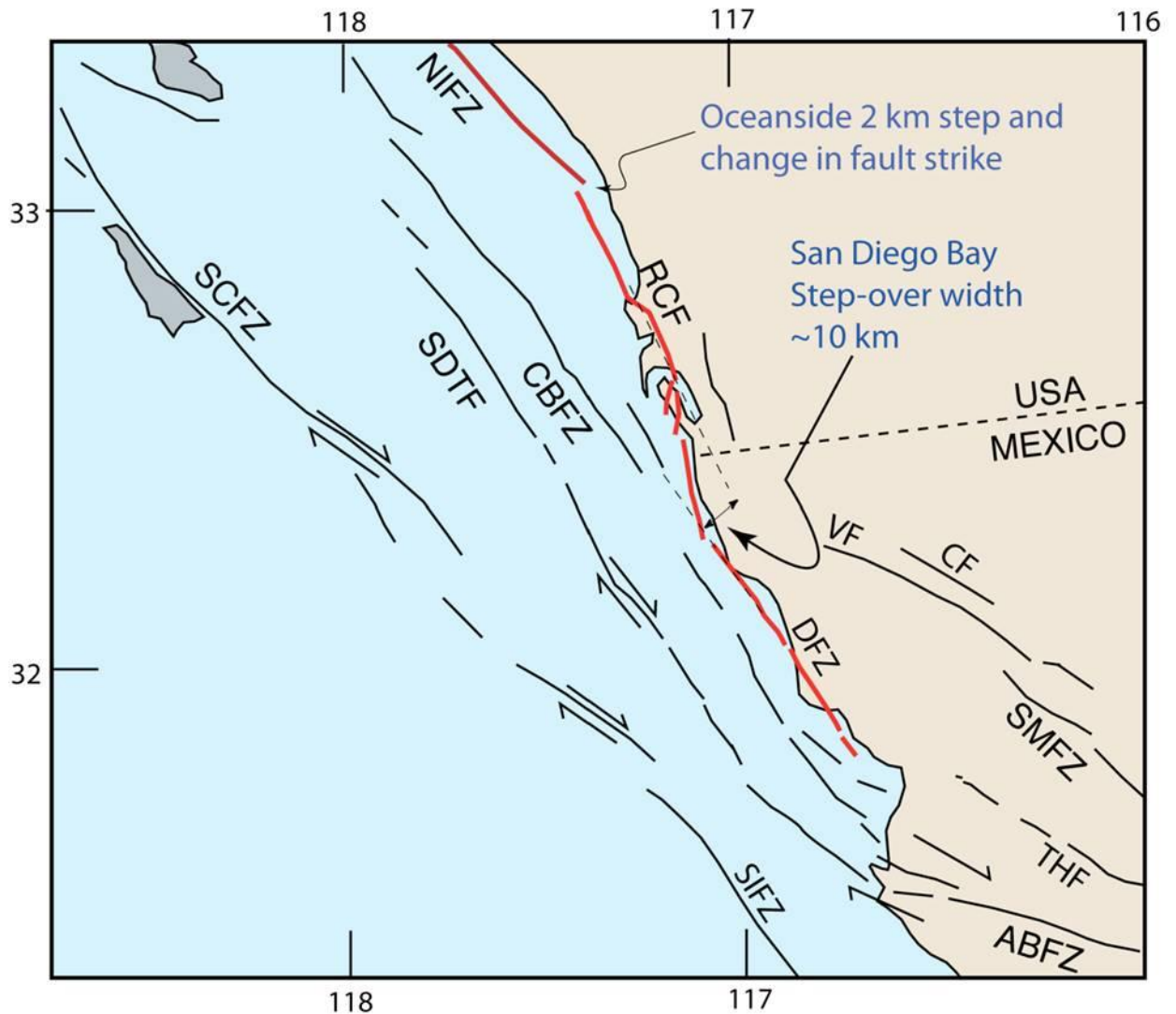
GeoPentech
Geotechnical & Geoscience Consultants

By Rockwell (2010)

**INTERPRETED 1941 AERIAL PHOTOGRAPHY
OF THE OLD TOWN AREA OF SAN DIEGO**

**FIGURE
A2-4**

SAN ONOFRE NUCLEAR GENERATING STATION
SEISMIC HAZARD ASSESSMENT PROGRAM



NOTE: Also shown is the smaller step at Oceanside with the change in fault strike. SAFZ - San Andreas fault zone; SJFZ - San Jacinto fault zone; IF - Imperial fault; CPF - Cerro Prieto fault; LSF - Laguna Salada fault; NIFZ - Newport- Inglewood fault zone; RCF - Rose Canyon fault; CF - Calabazas fault; VF - Vallecitos fault; SMFZ - San Miguel fault zone; THF - Tres Hermanes fault; ABFZ - Agua Blanca fault zone; CBFZ - Coronado Bank fault zone; DFZ - Descanso fault zone; SDTF - San Diego Trough fault; SCFZ - San Clemente fault zone; SIFZ - San Isidro fault zone.



GeoPentech
Geotechnical & Geoscience Consultants

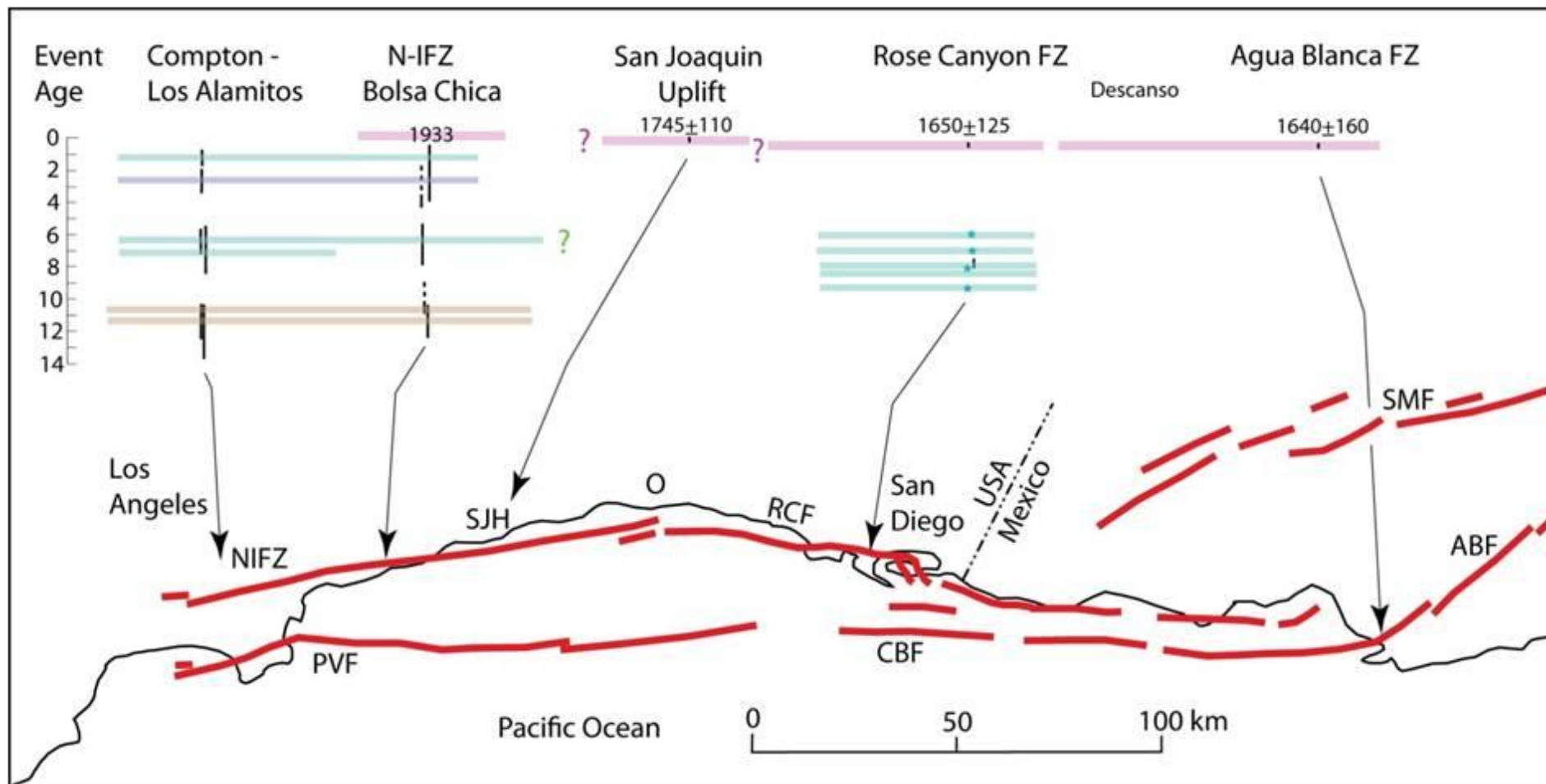
By Rockwell (2010)

**MAP SHOWING HOW STEP-OVER WIDTH WAS
MEASURED FOR THE SAN DIEGO BAY STEP**

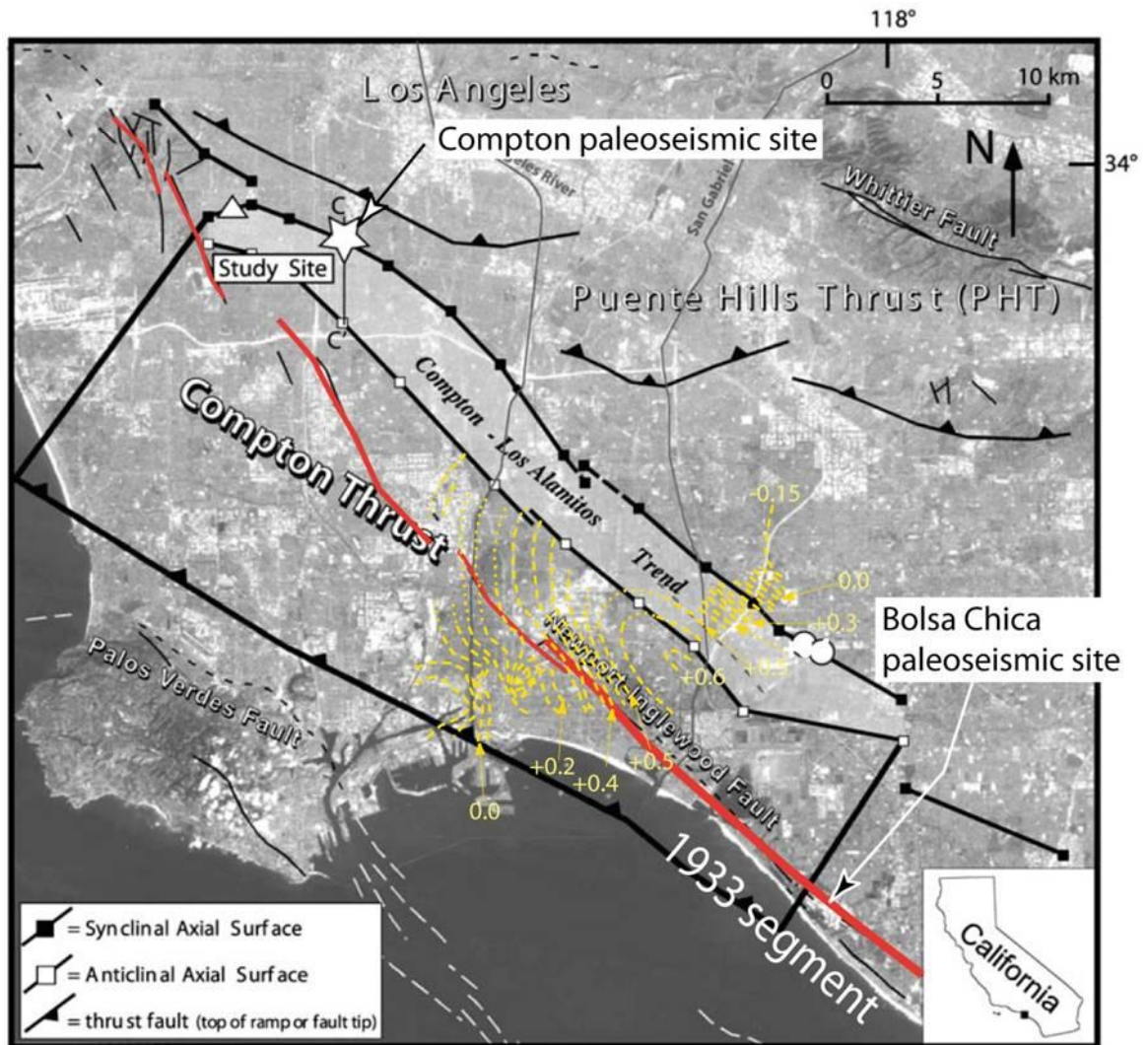
**FIGURE
A2-5**

SAN ONOFRE NUCLEAR GENERATING STATION

SEISMIC HAZARD ASSESSMENT PROGRAM



NOTE: Results from paleoseismic studies for the Agua Blanca, Rose Canyon, San Joaquin Hills, Newport-Inglewood, and Compton faults (from Grant and Rockwell, 2002; Grant et al., 1997, Leon et al., 2009).



NOTE: Location figure from Leon et al. (2009), showing their Compton paleoseismic site. The bolded red line is the inferred segment that ruptured in 1933 (Barrows, 1974), along with the area that sustained uplift in the 1933 earthquake, based on leveling data (Barrows, 1974). Maximum uplift was documented as more than 60 cm, with the locus between the Newport-Inglewood and Los Alamitos structures, supporting Wright's (1991) interpretation that the Compton-Los Alamitos trend is deformation associated with an oblique, high-angle fault.



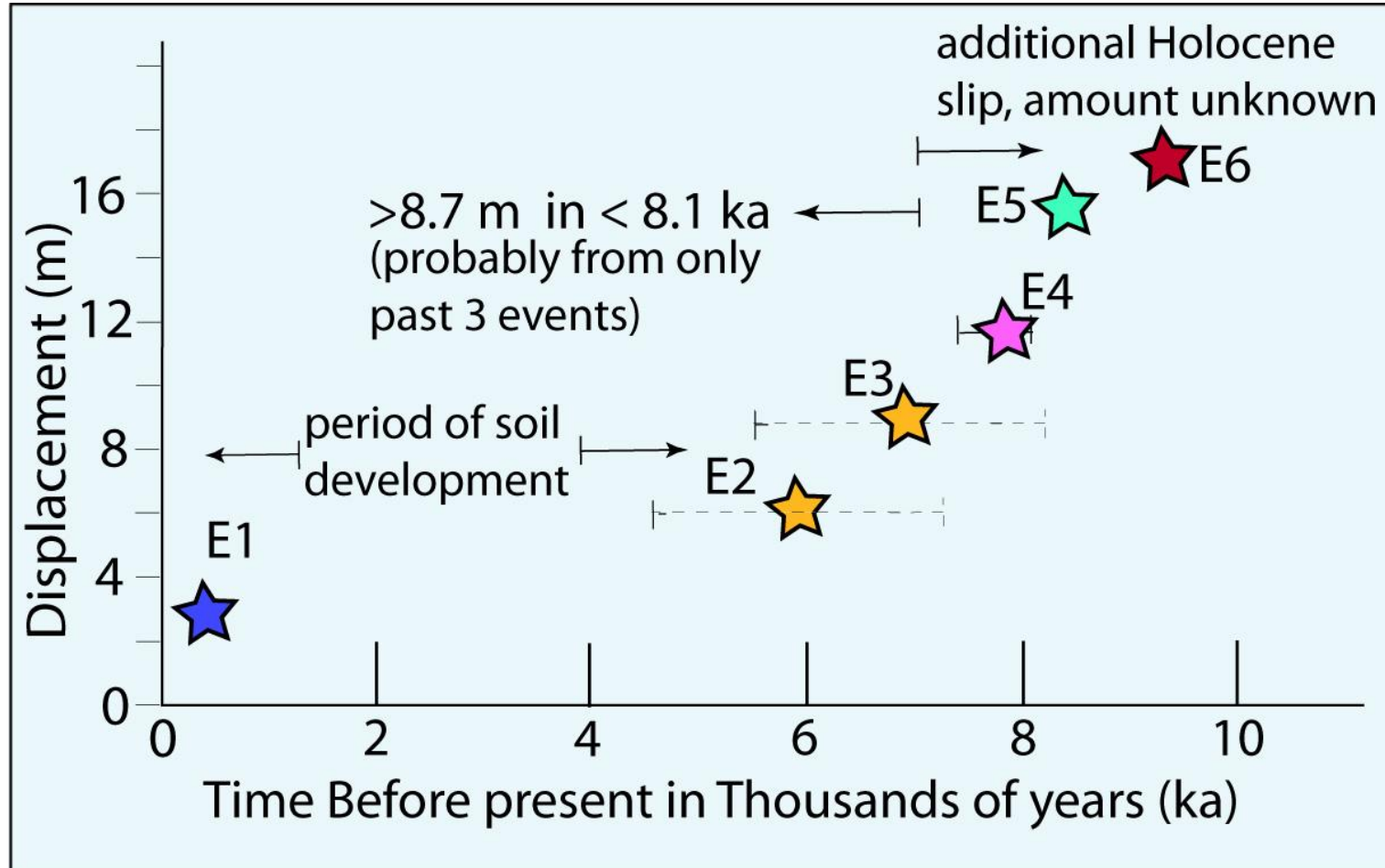
GeoPentech
Geotechnical & Geoscience Consultants

By Rockwell (2010)

LOCATION FIGURE FROM LEON ET AL. (2009)

FIGURE
A2-7

SAN ONOFRE NUCLEAR GENERATING STATION
SEISMIC HAZARD ASSESSMENT PROGRAM



NOTE: Timing of surface ruptures at Rose Creek, assuming that the strong soil development across the early Holocene fault splays accurately represents a lack of activity for several thousand years (from Rockwell, 2010a).



NOTE: GPS velocity field of the southern California Borderland, plotted with San Clemente Island as the reference frame (plotted in 2005 from the SCIGN web page).



GeoPentech
Geotechnical & Geoscience Consultants

By Rockwell (2010)

GPS VELOCITY FIELD OF THE SOUTHERN CALIFORNIA BORDERLAND

FIGURE
A2-9

SAN ONOFRE NUCLEAR GENERATING STATION
SEISMIC HAZARD ASSESSMENT PROGRAM

APPENDIX A – ATTACHMENT A-3

**SEISMIC SOURCE CHARACTERISTICS OF
INNER CALIFORNIA BORDERLAND'S BLIND THRUST FAULT SYSTEMS**

By

Dr. John Shaw and Dr. Andreas Plesch

Department of Earth and Planetary Sciences Harvard University, Cambridge, MA

INTRODUCTION

The following document has been prepared at the request of Southern California Edison (SCE) in consultation with technical members of their Seismic Hazard Assessment Program (SHAP).

Active thrust faults have long been known to exist in southern California, particularly in the Transverse Range Province. Awareness of the seismic risk associated with these thrust faults was heightened by the 1971 San Fernando (M_w 6.6) Earthquake, which resulted from slip on the San Fernando segment of the Sierra Madre Thrust Fault System; slip that ruptured the ground surface. Later, the 1987 Whittier Narrows (M_L 5.9) and the 1994 Northridge (M_w 6.7) earthquakes demonstrated the seismic hazards posed by these 'blind' thrust faults; slip that does not rupture the ground surface. The lack of surface ruptures on 'blind' thrust faults hinders our ability to locate them and assess their level of seismic activity.

The reverse/thrust focal mechanism solution tied to the offshore 1986 Oceanside (M_L 5.3) Earthquake demonstrated that active blind thrust faults also exist in southern California's Inner Continental Borderland. This offshore earthquake, combined with our extensive research of hundreds of proprietary oil industry marine geophysical seismic reflection survey lines, lead us to infer the presence of two distinct, active thrust fault systems located offshore of southern Orange County and San Diego County (Rivero et.al., 2000). As shown on Figure A3-1, the Oceanside Blind Thrust (OBT) extends at least from Laguna Beach to the Mexican border and may dip under the shoreline. The smaller Thirty-mile Bank Blind Thrust (TMBT) lies to the west, farther offshore.

Following is a brief discussion of our current understanding of the seismic source characteristic of the OBT and the TMBT developed since Rivero et.al. (2000). This briefing also summaries our current understanding of the relationship between the OBT and the TMBT with other thrust, reverse, normal, and strike-slip faults in southern California's Inner Continental Borderland. Most of what is presented herein is derived from what has been described in Rivero (2004) and Rivero and Shaw (in press).

Specifically, in this briefing we summarize:

- 1) Constraints on the location of the OBT and TMBT and our assessment of their level of seismic activity;
- 2) Our current understanding and weightings of the seismic characteristics of these two fault systems;

- 3) The logic tree developed to facilitate incorporating, particularly the OBT fault systems into SCE's Probabilistic Seismic Hazard Assessment (PSHA) and Probabilistic Tsunami Hazard Assessment (PTHA) updates for the San Onofre Nuclear Generating Station (SONGS);
- 4) The key remaining uncertainties regarding each fault's seismic source characteristics; and
- 5) Our recommendations for future efforts to resolve these key remaining uncertainties. A list of the references flagged herein is included at the end of this briefing document.

PRESENCE AND LEVEL OF ACTIVITY

In Rivero (2004) and Rivero and Shaw (in press) we supplemented the information provided in Rivero et.al., (2000) with more details on the various data supporting the presence and activity of the OBT and TMBT and their connections with the offshore high-angle, strike slip faults; the latter including the Newport-Inglewood (NI), Rose Canyon (RC), and San Diego Trough (SDT) faults.

These data include:

- a) High-resolution seismic reflection data that image the OBT and TMBT. These faults are defined by deep, shallow dipping, seismic reflections off the coast of southern California underlying folded and faulted sediments. The youngest of these sediments are inferred to be at least Plio-Pleistocene in age (some apparently displacing the sea floor).
- b) Balanced and restored cross sections that document significant contraction or shortening on these structures since the Pliocene (such as the ~2.2 to 2.7 km across the OBT within the last ~1.8 – 2.4 million years).
- c) Earthquake epicenter/hypocenter/focal mechanisms, particularly the Oceanside 1986 M_L 5.3 event, which occurred between San Clemente Island and Oceanside, CA and ruptured the TMBT. In addition, the 1986 Coronado Bank earthquake events, max M_L 3.7, which occurred offshore of Point Loma in August 1986 (Astiz and Shearer, 2000), were incorporated in our analysis;
- d) Elevated marine terraces along the Orange/San Diego County's shoreline; and
- e) GPS data from the SCEC Crustal Motion Map that Kier and Mueller (1999) used to calculate the components of motion perpendicular to the offshore thrust fault traces. Rivero 2005 used the maximum of these station values, minus the slip rate derived for the OBT, to bracket the slip rate on the Thirty-mile Bank fault. Our sense is that these geodetic data are poorly constrained, largely due to the lack of offshore data coverage. Thus, there is a large uncertainty associated with this rate determination, but at present we simply lack another means to estimate this rate.

SEISMIC CHARACTERISTICS

Figure A3-1 provides a map of the OBT and TMBT and their associated hanging wall and footwall subsidiary faults, as modified from Rivero (2004). Also modified from Rivero (2004), Figure A3-2 summarizes the various rupture models considered for these faults. Figure A3-3 provides a more simplified version of the fault map presented on Figure A3-1. This more simplified map was used to obtain the representative three dimensional coordinates for the OBT, TMBT and their associated splay faults relative to the location of the SONGS for input into the PSHA program (Abrahamson, 2010).

The table presented in Figure A3-4 provides a complete listing of our current estimates of the OBT's and TMBT's seismic source characteristics. In addition, we provide seismic source characteristics of other thrust, reverse, normal, and strike-slip faults in the region that may rupture in conjunction with the OBT and TMBT Fault Systems. Each row of the table represents different individual or multi-segment combinations of plausible rupture scenarios, keyed to the schematic drawings of the four alternative rupture models presented in Figure A3-2.

The rupture area (km²) for each plausible rupture scenario listed in Figures A3-3 and A3-4 was estimated based on the 3-D mapping of the fault in the SCEC Community Fault Model that we have developed (Plesch et al., 2007), assuming a seismogenic depth > 5 km and <17 km. The resulting maximum magnitude earthquake was then calculated using the rupture area versus magnitude relationships developed by Wells and Coppersmith (1994).

The slip rate was estimated for the OBT based on measures of fault offsets and uplift using the marine geophysical seismic reflection survey data and estimates of the ages of the deformed geologic formations. Using the estimated slip rates we then calculated recurrence intervals of the maximum magnitude earthquake for each particular rupture scenario using Wells & Coppersmith (1994) and Shaw and Suppe (1996).

The slip rate for the TMBT was estimated from limited GPS data, as discussed above. We have no constraints on the slip rate of the SDT fault, although it appears to be active based on offsets of near seafloor horizons.

The slip rate on the Carlsbad Fault was estimated by Rivero (2004) based on a range of dip-slip values (0.4 to 0.6 km) using two alternative structural models. The rates are derived using maximum and minimum ages (2.4 and 1.8 mya, respectively) for the initiation of faulting and folding, as defined by patterns of syntectonic (growth) sediments.

Slip rate estimates for the offshore extensions of the NI and RC right-lateral strike-slip faults were based on slip rates assigned to the on-shore traces of these faults from CGS (2002).

LOGIC TREE FOR PSHA/PTHA

Our sense is that these alternative rupture models represent a range of possible scenarios. In reality, however, some may not occur. If more than 1 of these alternatives does occur (which seems plausible), it implies that various fault segment rupture in different types of earthquakes. Thus, the alternatives attempt to capture both epistemic and aleatory uncertainty.

The first step in utilizing the above seismic source characterization of the OBT, TMBT and related subsidiary faults in the SONGS PSHA involved the preparation of the logic tree presented on Figure A3-5. This logic tree was used to accommodate both the epistemic and aleatory uncertainty in the seismic source characteristics (SSC) of the various alternative rupture models. A digital file of this logic tree is also provided in the attached CD.

In terms of our confidence in the reality of the various branches of the logic tree presented on Figure A3-5, we feel it is acceptable to apply equal weights to accommodate the epistemic uncertainty in both model 3 and 4, and a reduced weight for model 2. Although this is a subjective assessment, we would suggest that model 2 should be weighted substantially lower than model 3 or 4 (by a factor 4 or more).

Our reasoning for this weighting is that no viable structural model has been presented to explain the observed slip on the Oceanside thrust is driven by motion on the strike-slip faults. Therefore on a percentage basis, in terms of our best guess, something like 45% for model 3, 45% for model 4, and 10% for model 2, would be a reasonable fit.

We recognize that others believe that right-lateral strike slip faults (model 1) dominate the tectonics off-shore of Orange and San Diego Counties. However, based on the currently available data, we would assign a weight of '0' to rupture model 1 on Figure A3-5. As we stated above, rupture model 1 is not kinematically compatible with the large amount of displacement we document on the OBT Fault. Thus, we believe that the seismogenic potential of the strike-slip faults is represented most effectively in models 2, 3, or 4.

Our percentage weightings applied to the alternative linkage hypotheses for both single and complex strike-slip and thrust earthquake sources in rupture models 3 and 4, are also shown on Figure A3-5. These best guess percentages also reflect on the current epistemic uncertainty of the existing data regarding the connection of the various possible rupture linkages within a seismogenic depth > 5 km and <17 km.

Based on the available data and interpretations there are 67 combinations of fault rupture segments as shown on Figure A3-5. Those branches of the logic tree that reflect the "either/or" epistemic uncertainty of the data are highlight with blue colored lines. The "sometime this way/ sometimes that way" aleatory uncertainty in the data is highlighted in the logic tree by orange line boxes.

Model 1 (0% weighting) focuses the remaining portion of this Appendix on the remaining three OBT models. The possibility of Model 1 as a likely seismic source is discussed in more detail in the other subsections of Appendix A.

Model 2 (10% weighting) reflects two separate alternative seismic sources, i.e., the high angle, strike-slip NI and RC faults. Either these two sources is reflected as 'sometimes' rupturing only on a single segment and 'sometimes' rupturing on multisegments, both onshore and offshore. Model 2 also accommodates the aleatory possibility that the OBT will rupture as a southwest vergent subsidiary fault off of either the NI or the RC faults' rupture. Using the magnitude and slip rate calculations listed in Figure A3-4, the resulting earthquake recurrence was calculated using the Wells and Coppersmith, (1994) Maximum Magnitude recurrence models.

Model 3 (45% weighting) reflects three separate alternative seismic sources, i.e., the onshore/near shore segments of the NI and RC strike-slip faults and the OBT. The OBT has two epistemic branches reflecting the uncertainty as to its extent on-shore to the north of Dana Point and under the San Joaquin Hills. This uncertainty impacts the source area/maximum magnitude calculation, but otherwise the make-up of the logic tree is the same for the branch "North of Dana Point" as is for the branch "South of Dana Point". Using the "South of Dana Point" branch as an example for Model 3, the 4 "linkage" options, i.e., 3a, 3b₁, 3b₂, and 3c and their corresponding epistemic weightings are considered. Then under each of these four linkage alternatives, the single and multiple thrust fault/hanging and footwall subsidiary fault aleatory randomness is accommodated. Then, as was explained in the Model 2 discussion, for each of these rupture models the corresponding slip rates and recurrence calculations are provided.

Model 4 (45% weighting) reflects a similar logic three as Model 3, but with fewer branches to reflect the lack of a footwall faults in Model 4 in comparison with Model 3. However, two differences exist between Model 3 and Model 4 rupture scenarios. The first of these differences is reflected by “linkage 4b” where no seismogenic links exist between the high-angle strike-slip fault in the hanging wall above the OBT because of its depth below the seismic zone (> 17 km). In this situation the hanging wall, high angle, strike-slip fault ruptures as an independent source in addition to the thrust fault source. The second Model 4 versus Model 3 variation was to accommodate the presence of the Carlsbad Thrust Fault in the hanging wall above the OBT. The Carlsbad fault rupture scenario was not part of Model 3 because its presence only in the hanging wall was clearly supported by the marine seismic reflection data, thus only fitting Model 4.

KEY REMAINING UNCERTAINTIES

The key uncertainties associated with representing these potential seismic sources in the SONGS’s PSHA result from the lack of good constraints on the fault slip rates and the inability to distinguish between the several single and multi-segment rupture scenarios that are considered. Specifically, it is unclear whether the shallow dipping thrust faults (such as the OBT) are the primary seismic source faults, with the steeply dipping, right-lateral, strike-slip faults, such as the NI or the RC faults, being subsidiary, or whether the steep, strike-slip faults are the primary seismic sources, and the thrust faults are subsidiary.

Unfortunately this uncertainty continues to exist. The TMBT fault is locally imaged in the seismic reflection to the east of its intersection of the San Diego Trough strike-slip fault. This, combined with the location and focal mechanism of the 1986 Oceanside earthquake, imply that the TMBT is a continuous, active structure. This favors models 3 and 4. None of the seismic reflection profiles we examined, however, clearly imaged subsurface conditions at the depths and locations necessary to resolve the critical interactions of the OBT and NI-RC system. The OBT is not imaged in these locations because it juxtaposes basement on top of basement rocks. Thus, no significant impedance boundary exists, and the fault cannot be imaged by the seismic data.

Regarding fault activity and slip rates, the TMBT is clearly active based on the 1986 Oceanside earthquake. However, its recent (Holocene) slip rate is largely unconstrained, as is the slip rate for the San Diego Trough strike-slip fault. We simply lack the ability to measure direct fault offsets and/or to have constraints on the ages of offset horizons given the lack of well data in this area. The evidences for activity of the OBT are more indirect. Perhaps the best constraints on recent activity of the OBT come from folded and offset horizons at or near the seafloor. However, lacking direct age control for these young sediments limits our ability to constrain how recently the fault has ruptured and its slip rate. Association of the OBT and the San Joaquin Hills thrust, combined with the patterns of uplifted coastal marine terraces, further support fault activity.

RECOMMENDATIONS TOWARDS RESOLVING REMAINING UNCERTAINTIES

At the depths and locations where data is necessary to resolve the uncertainty discussed above regarding the intersection between the NI/RC and the OBT, the faults are within the basement rocks and the velocity contrast/acoustic impedance of the basement rocks either side of where these faults are inferred to be interfacing is not likely to be significant enough to produce adequate reflectors in the marine geophysical seismic reflection surveys. As such, even if environmental hurdles to future deep seismic surveys are overcome, it is doubted whether high energy, deep penetrating 2-D or 3-D seismic

**SAN ONOFRE NUCLEAR GENERATING STATION
SEISMIC HAZARD ASSESSMENT PROGRAM
2010 PROBABILISTIC SEISMIC HAZARD ANALYSIS REPORT**

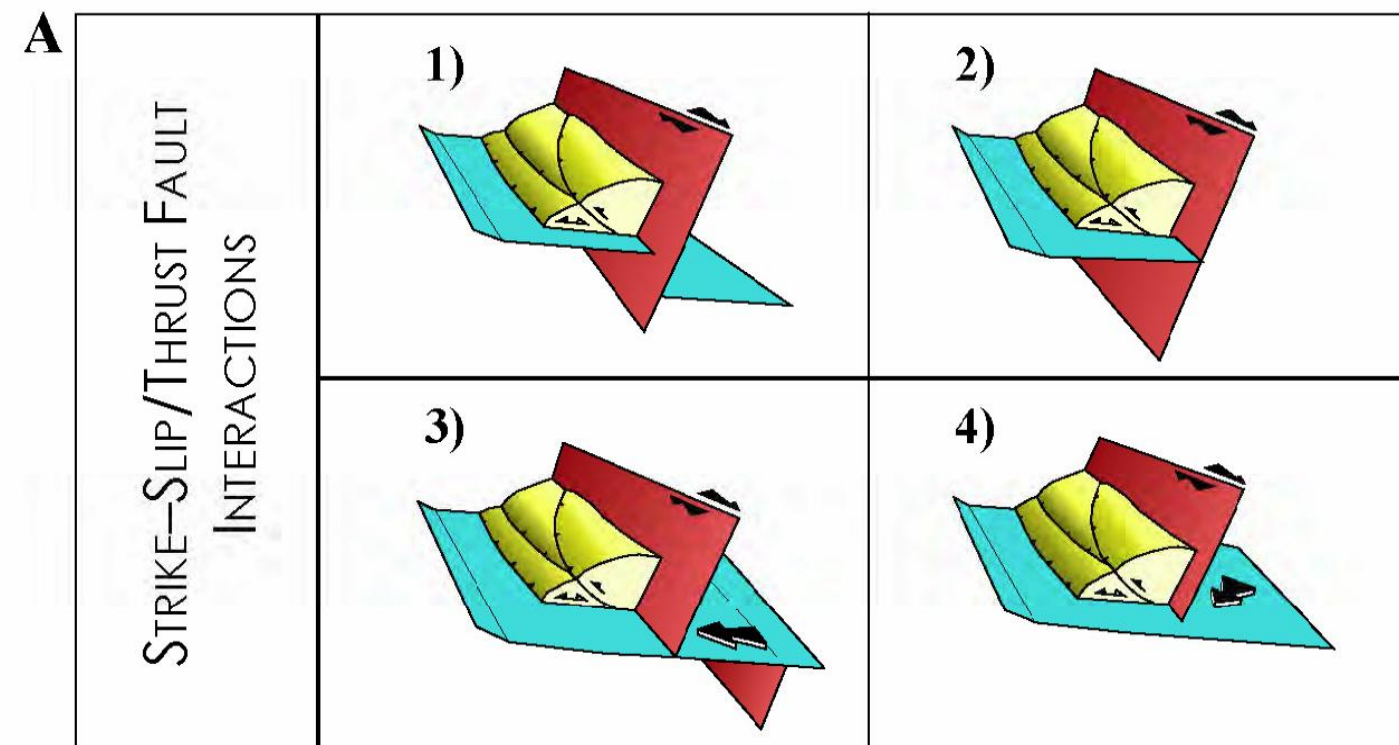
surveys can retrieve the necessary data to be able to unequivocally resolve this particularly important uncertainty.

In lieu of this data, the following is recommended to better define the extent of the OBT and the TMBT and to more precisely estimate their late Pleistocene and Holocene activity.

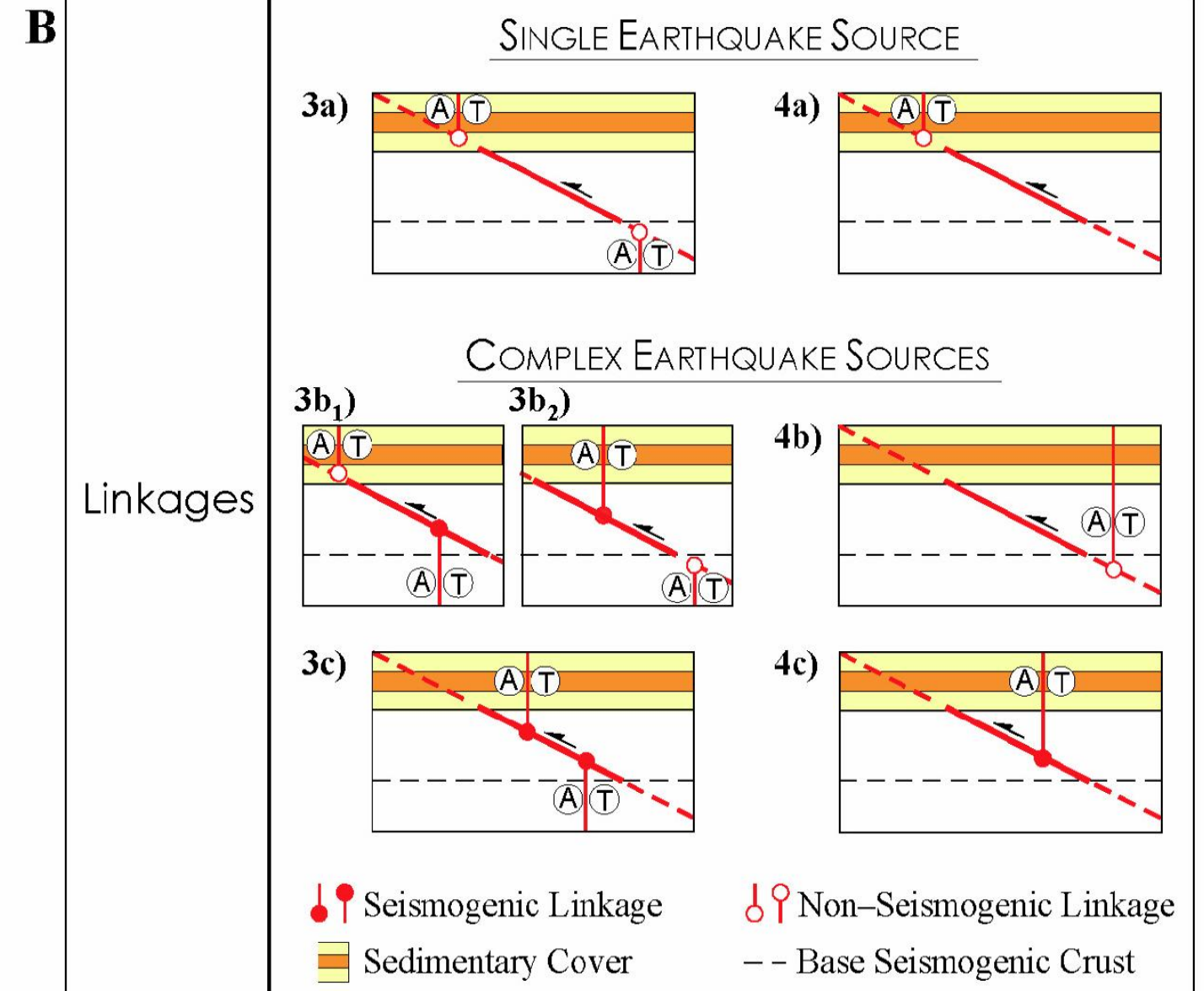
- High-resolution side-scan sonar and seismic reflection imaging of seafloor deformation combined with sediment sampling and dating, would likely provide better constraints on activity and slip rates for the OBT, TMBT, and San Diego Trough strike-slip fault (highest priority). Regarding recommended sites of future studies, Figure A3-6 highlights three possible study regions. Clearly, we would need to do a more thorough evaluation of current data to confirm the appropriateness of each site, and the particular types of data (side-scan sonar, high-res seismic) that would be most useful. Nevertheless, region 1 would target improving our understanding of the along strike continuity of the Oceanside and San Joaquin Hills structures, as well as the offshore Newport-Inglewood fault. Region 2 would target defining a slip rate on the Carlsbad fault based on the discrete near-surface fold, as well as perhaps a slip rate on the offshore Rose Canyon fault system. Region 3 would target the San Diego Trough fault in a releasing bend, thereby constraining the fault slip rate.
- Precise relocation of offshore seismicity using newly available 3D velocity models for the region and advanced relocation methods. Better earthquake locations will improve our ability to establish which fault segments are active, and to define better their subsurface geometries.
- Evaluation of current geodetic observations to improve constraints on shortening and strike-slip rates.

REFERENCES

- Abrahamson, Norm A. (personal communication, 2010)
- Astiz, Luciana, and Shearer, Peter (2000). Earthquake Locations in the Inner Continental Borderland, Offshore Southern California, *Bulletin of the Seismological Society of America*, v. 90, no. 2. 425-449.
- California Geological Survey (2002). California fault parameters-Interactive fault parameter map of California,
http://www.consrv.ca.gov/cgs/rghm/psha/fault_parameters/htm/Pages/index.aspx.
- Kier, Grant, and Mueller, Karl (1999). Flexural modeling of the northern Gulf of California Rift: Relating marine terrace uplift to the forebulge on a subsiding plate, *Southern California Earthquake Center 1999 internship final report*, 11p.
- Plesch, Andreas, et. al. (2007). Community Fault Model (CFM) for Southern California, *Bulleting of the Seismological Society of America*, v. 97, no. 6, 1793-1802.
- Rivero, Carlos, et. al. (2000). Oceanside and Thirty-mile Bank blind thrusts: Implications for earthquake hazards in coastal southern California, *Geology*, v. 28, no. 10, 891-894.
- Rivero-Ramirez, Carlos Alberto (2004). Origin of Active Blind-Thrust Faults in the southern Inner California Borderlands, thesis, *Department of Earth and Planetary Sciences, Harvard University, Cambridge, Massachusetts*, 176 p.
- Rivero, Carlos, and Shaw, John H. (2005). Fault related folding in reactivated offshore basins, California, *Interpretation of Contractional Fault-Related Folds, An AAPG Seismic Atlas, Studies in Geology*, no. 53, 3 p.
- Rivero, Carlos, and Shaw, John H. (in press). Active Folding and Blind-thrust Fault Induced by Basin Inversion Processes, Inner California Borderlands, *AAPG*.
- Shaw, John H. and Suppe, John (1996). Earthquake Hazards of Active Blind-thrust Faults Under the Central Los Angeles Basin, California: *Journal of Geophysical Research* 101, B4, p. 8623-8642.
- Wells, D.L., and Coppersmith, K. J., (1994). New empirical relationships among the Magnitude, Rupture Length, Rupture Width, Rupture Area, and Surface Displacement: *Bulletin of the Seismological Society of America*, v. 84, p. 974-1002.

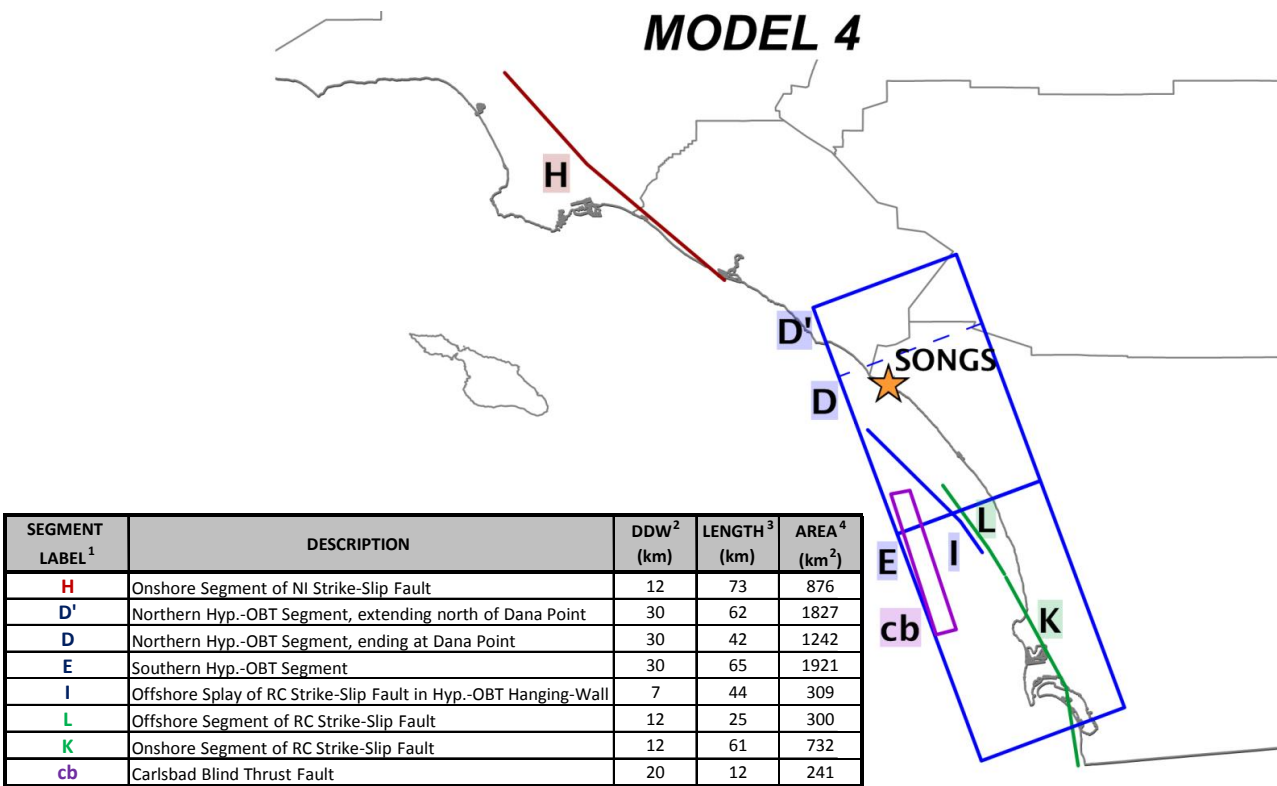
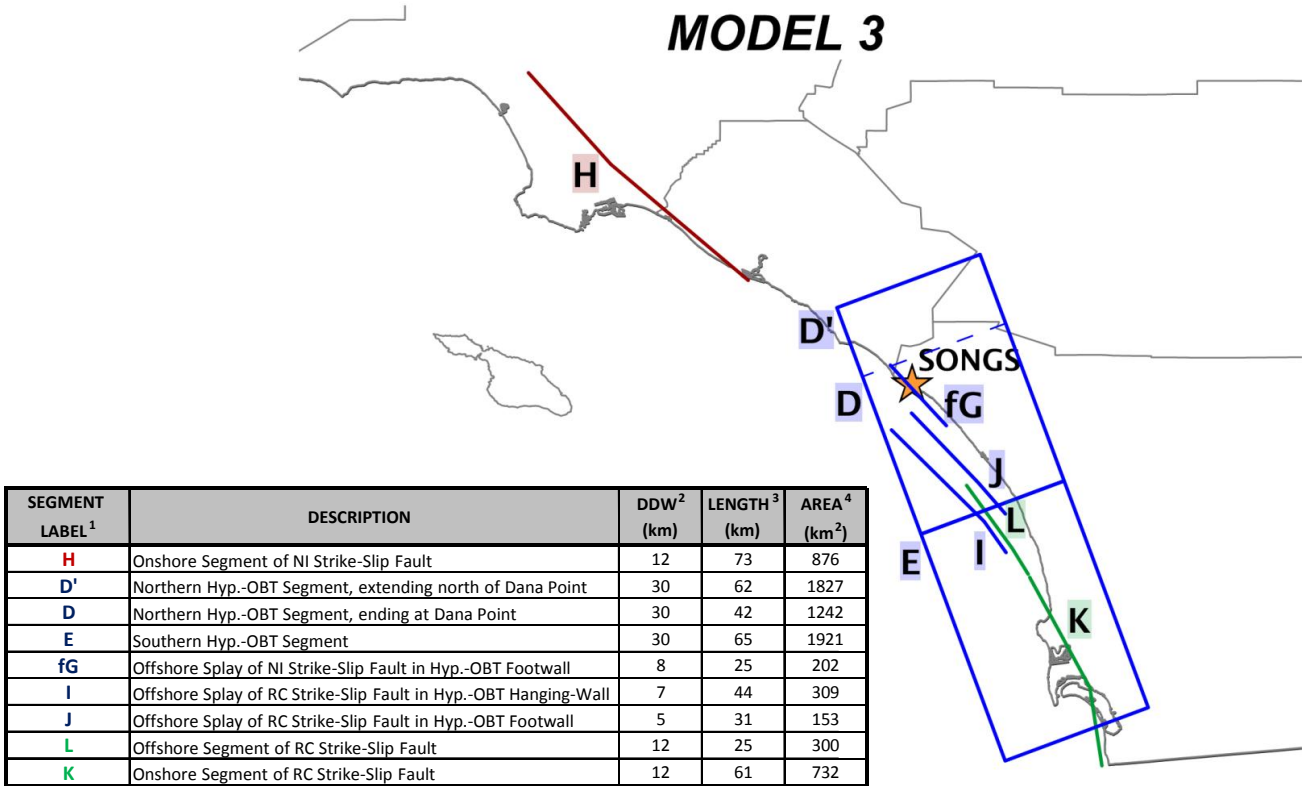
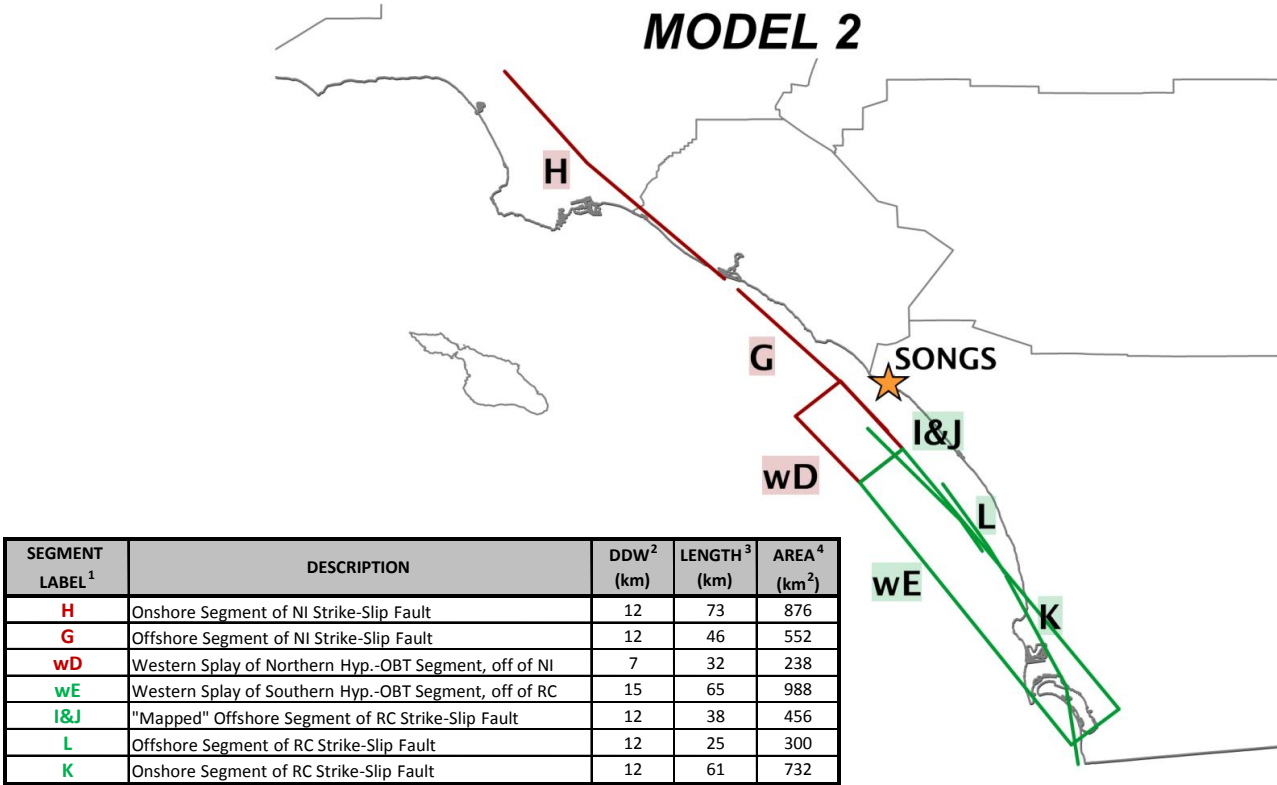
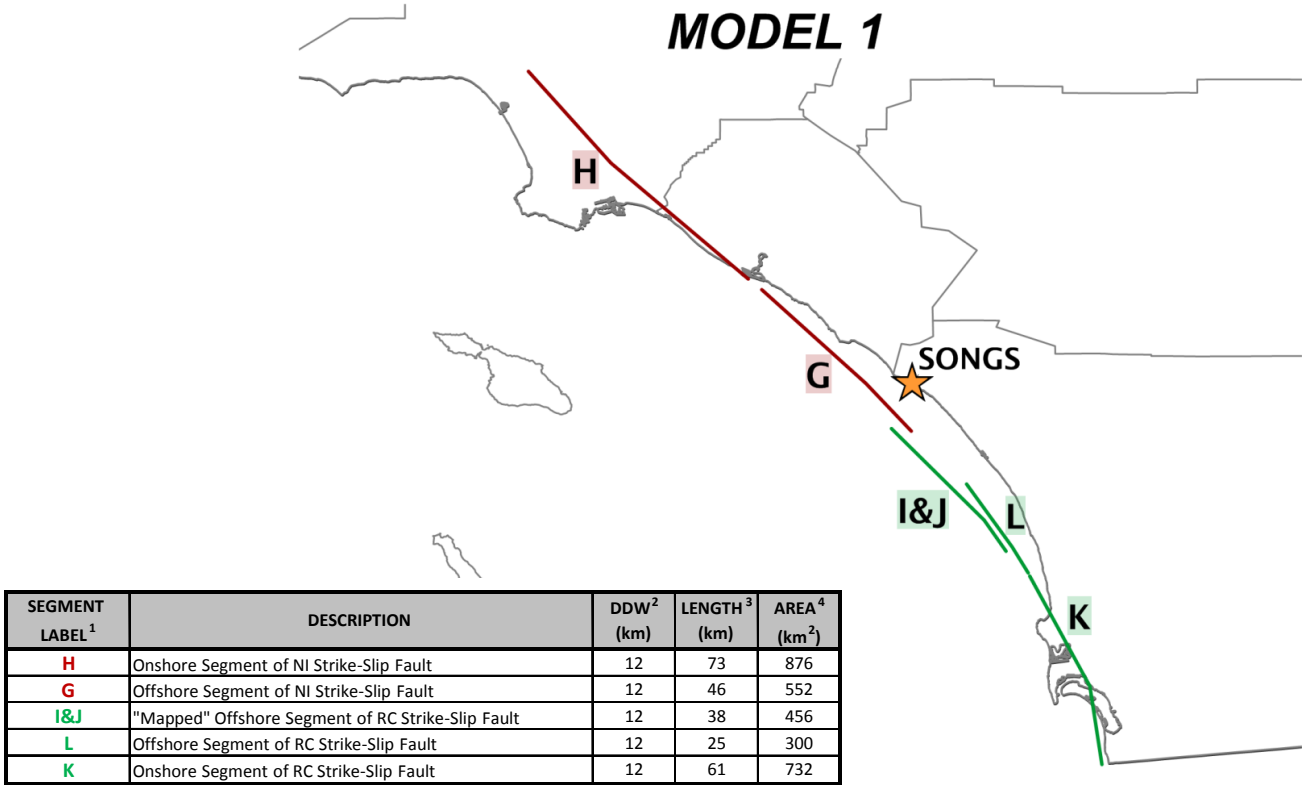


- 3a) NON-SEISMOGENIC LINKAGES WITH 1 EARTHQUAKE SOURCE
- 3b) HYBRID SEISMOGENIC LINKAGES WITH 2 EARTHQUAKE SOURCES
- 3c) SEISMOGENIC LINKAGES WITH 3 EARTHQUAKE SOURCES
- 4a) NON-SEISMOGENIC LINKAGE WITH 1 EARTHQUAKE SOURCE
- 4b) NON-SEISMOGENIC LINKAGE WITH 2 EARTHQUAKE SOURCES
- 4c) SEISMOGENIC LINKAGE WITH 2 EARTHQUAKE SOURCES



(A) Schematic representation of different structural scenarios considered in this study for strike-slip and blind-thrust fault interactions [modified from Rivero *et al.*, 2000]. (B) Geometric linkages between strike-slip and blind-thrust faults defined for preferred structural scenarios 3.25A₃ and 3.25A₄. The type of geometric linkage and their position relative to the depth of the sediments and the seismogenic crust determine the seismogenic potential of the faults and the type of earthquake source.

Notes: Modified from Rivero (2004)





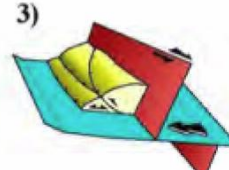

Notes:

¹ Labels modified from Figure A-2-1

² Assuming 5km to 17km Seismogenic Depth

³ Based on Rivero (2004)

⁴ Calculated based on DDW and Length


| KINEMATIC MODEL | SEISMIC SOURCE | OBT LIMIT | LINKAGE | SINGLE SEGMENT | | | | | MULTI SEGMENT | | | | |
|---|------------------|----------------------------------|---------|----------------|---------------------------------|--------------------------|--------------------------------|-----------------------------|----------------|---------------------------------|--------------------------|--------------------------------|-----------------------------|
| | | | | SEGMENTS | RUPTURE AREA (KM ²) | MAX MAG ¹ (M) | SLIP RATE ² (mm/yr) | RECURRENT ³ (yr) | SEGMENTS | RUPTURE AREA (KM ²) | MAX MAG ¹ (M) | SLIP RATE ² (mm/yr) | RECURRENT ³ (yr) |
|  | NI Strike-Slip | | | G | 552 | 6.8 | 1.5+/-0.5 | 390 - 780 | G + H | 1428 | 7.2 | 1+/-0.5 | 980 - 2940 |
| | | | | H | 876 | 7.0 | 1+/-0.5 | 710 - 2140 | | | | | |
| | RC Strike-Slip | | | I&J | 456 | 6.7 | 1.07+/-0.03 | 600 - 640 | I&J + K | 1188 | 7.1 | 1.07+/-0.03 | 1140 - 1210 |
| | | | | K | 732 | 6.9 | 1.07+/-0.03 | 830 - 880 | K + L | 1032 | 7.0 | 1.07+/-0.03 | 970 - 1030 |
| | | | | L | 300 | 6.5 | 1.07+/-0.03 | 440 - 470 | L + I&J | 756 | 6.9 | 1.07+/-0.03 | 830 - 880 |
| | | | - | - | - | - | - | - | I&J + K + L | 1488 | 7.2 | 1.07+/-0.03 | 1340 - 1420 |
|  | NI Strike-Slip | | | G&wD | 790 | 6.9 | 1.02+/-0.14 | 790 - 1040 | G&wD + H | 1666 | 7.2 | 1.02+/-0.14 | 1270 - 1670 |
| | | | | H | 876 | 7.0 | 1+/-0.5 | 710 - 2140 | | | | | |
| | RC Strike-Slip | | | I&J&wE | 1444 | 7.2 | 0.82+/-0.12 | 1570 - 2100 | I&J&wE + K | 2176 | 7.3 | 0.82+/-0.12 | 1840 - 2470 |
| | | | | K | 732 | 6.9 | 1.07+/-0.03 | 830 - 880 | K + L | 1032 | 7.0 | 1.07+/-0.03 | 970 - 1030 |
| | | | | L | 300 | 6.5 | 1.07+/-0.03 | 440 - 470 | L + I&J&wE | 1744 | 7.2 | 0.82+/-0.12 | 1570 - 2100 |
| | | | - | - | - | - | - | - | I&J&wE + K + L | 2476 | 7.4 | 0.82+/-0.12 | 2150 - 2890 |
|  | NI Strike-Slip | | | H | 876 | 7.0 | 1+/-0.5 | 710 - 2140 | - | - | - | - | - |
| | RC Strike-Slip | | | K | 732 | 6.9 | 1.07+/-0.03 | 830 - 880 | K + L | 1032 | 7.0 | 1.07+/-0.03 | 970 - 1030 |
| | Oceanside Thrust | Ends at Dana Point (D) | 3a | D | 1242 | 7.1 | 1.02+/-0.14 | 1080 - 1430 | D + E | 3163 | 7.5 | 1.02+/-0.14 | 2040 - 2690 |
| | | | | E | 1921 | 7.3 | 0.82+/-0.12 | 1840 - 2470 | | | | | |
| | | | 3b1 | D&fG | 1444 | 7.2 | 1.02+/-0.14 | 1270 - 1670 | D&fG + E&J | 3518 | 7.6 | 1.74+/-0.2 | 1430 - 1810 |
| | | | | E&J | 2074 | 7.3 | 0.82+/-0.12 | 1840 - 2470 | | | | | |
| | | | 3b2 | D | 1242 | 7.1 | 1.02+/-0.14 | 1080 - 1430 | D + E&I | 3472 | 7.5 | 1.74+/-0.2 | 1220 - 1540 |
| | | | | E&I | 2230 | 7.4 | 0.82+/-0.12 | 2150 - 2890 | | | | | |
| | | | 3c | D&fG | 1444 | 7.2 | 1.02+/-0.14 | 1270 - 1670 | D&fG + E&I&J | 3827 | 7.6 | 1.74+/-0.2 | 1430 - 1810 |
| | | | | E&I&J | 2383 | 7.4 | 0.82+/-0.12 | 2150 - 2890 | | | | | |
| | Oceanside Thrust | Extends North of Dana Point (D') | 3a | D' | 1827 | 7.3 | 1.02+/-0.14 | 1490 - 1960 | D' + E | 3748 | 7.6 | 1.02+/-0.14 | 2400 - 3160 |
| | | | | E | 1921 | 7.3 | 0.82+/-0.12 | 1840 - 2470 | | | | | |
| | | | 3b1 | D'&fG | 2029 | 7.3 | 1.02+/-0.14 | 1490 - 1960 | D'&fG + E&J | 4103 | 7.6 | 1.74+/-0.2 | 1430 - 1810 |
| | | | | E&J | 2074 | 7.3 | 0.82+/-0.12 | 1840 - 2470 | | | | | |
| | | | 3b2 | D' | 1827 | 7.3 | 1.02+/-0.14 | 1490 - 1960 | D' + E&I | 4057 | 7.6 | 1.74+/-0.2 | 1430 - 1810 |
| | | | | E&I | 2230 | 7.4 | 0.82+/-0.12 | 2150 - 2890 | | | | | |
| | | | 3c | D'&fG | 1444 | 7.2 | 1.02+/-0.14 | 1270 - 1670 | D'&fG + E&I&J | 4412 | 7.6 | 1.74+/-0.2 | 1430 - 1810 |
| | | | | E&I&J | 2383 | 7.4 | 0.82+/-0.12 | 2150 - 2890 | | | | | |
|  | NI Strike-Slip | | | H | 876 | 7.0 | 1+/-0.5 | 710 - 2140 | - | - | - | - | - |
| | RC Strike-Slip | | | K | 732 | 6.9 | 1.07+/-0.03 | 830 - 880 | K + L | 1032 | 7.0 | 1.07+/-0.03 | 970 - 1030 |
| | Oceanside Thrust | Ends at Dana Point (D) | 4b | D | 1242 | 7.1 | 1.02+/-0.14 | 1080 - 1430 | D + E | 3163 | 7.5 | 1.02+/-0.14 | 2040 - 2690 |
| | | | | E | 1921 | 7.3 | 0.82+/-0.12 | 1840 - 2470 | | | | | |
| | | | | I | 309 | 6.5 | 1.07+/-0.03 | 440 - 470 | | | | | |
| | | | 4c | D | 1242 | 7.1 | 1.02+/-0.14 | 1080 - 1430 | D + E&I | 3472 | 7.5 | 1.74+/-0.2 | 1220 - 1540 |
| | | | | E&I | 2230 | 7.4 | 0.82+/-0.12 | 2150 - 2890 | | | | | |
| | | Extends North of Dana Point (D') | 4b | D' | 1827 | 7.3 | 1.02+/-0.14 | 1490 - 1960 | D' + E | 3748 | 7.6 | 1.02+/-0.14 | 2400 - 3160 |
| | | | | E | 1921 | 7.3 | 0.82+/-0.12 | 1840 - 2470 | | | | | |
| | | | | I | 309 | 6.5 | 1.07+/-0.03 | 440 - 470 | | | | | |
| | | | 4c | D' | 1827 | 7.3 | 1.02+/-0.14 | 1490 - 1960 | D' + E&I | 4057 | 7.6 | 1.74+/-0.2 | 1430 - 1810 |
| | | | E&I | 2230 | 7.4 | 0.82+/-0.12 | 2150 - 2890 | | | | | | |
| Carlsbad Thrust | | | cb | 241 | 6.4 | 0.25+/-0.08 | 1250 - 2430 | - | - | - | - | - | |

Notes:

¹Maximum Magnitude based on Wells & Coppersmith (1994)

²Value estimated by Rivero (2004) or Shaw & Plesch (2010)

³Recurrence Interval based on Shaw & Suppe (1996)



GeoPentech

Geotechnical & Geoscience Consultants

By Shaw and Plesch (2010)

SAN ONOFRE NUCLEAR GENERATING STATION

SEISMIC HAZARD ASSESSMENT PROGRAM

POTENTIAL RUPTURE SCENARIOS

FOR BLIND THRUST AND RIGHT LATERAL STRIKE-SLIP SYSTEMS

FIGURE

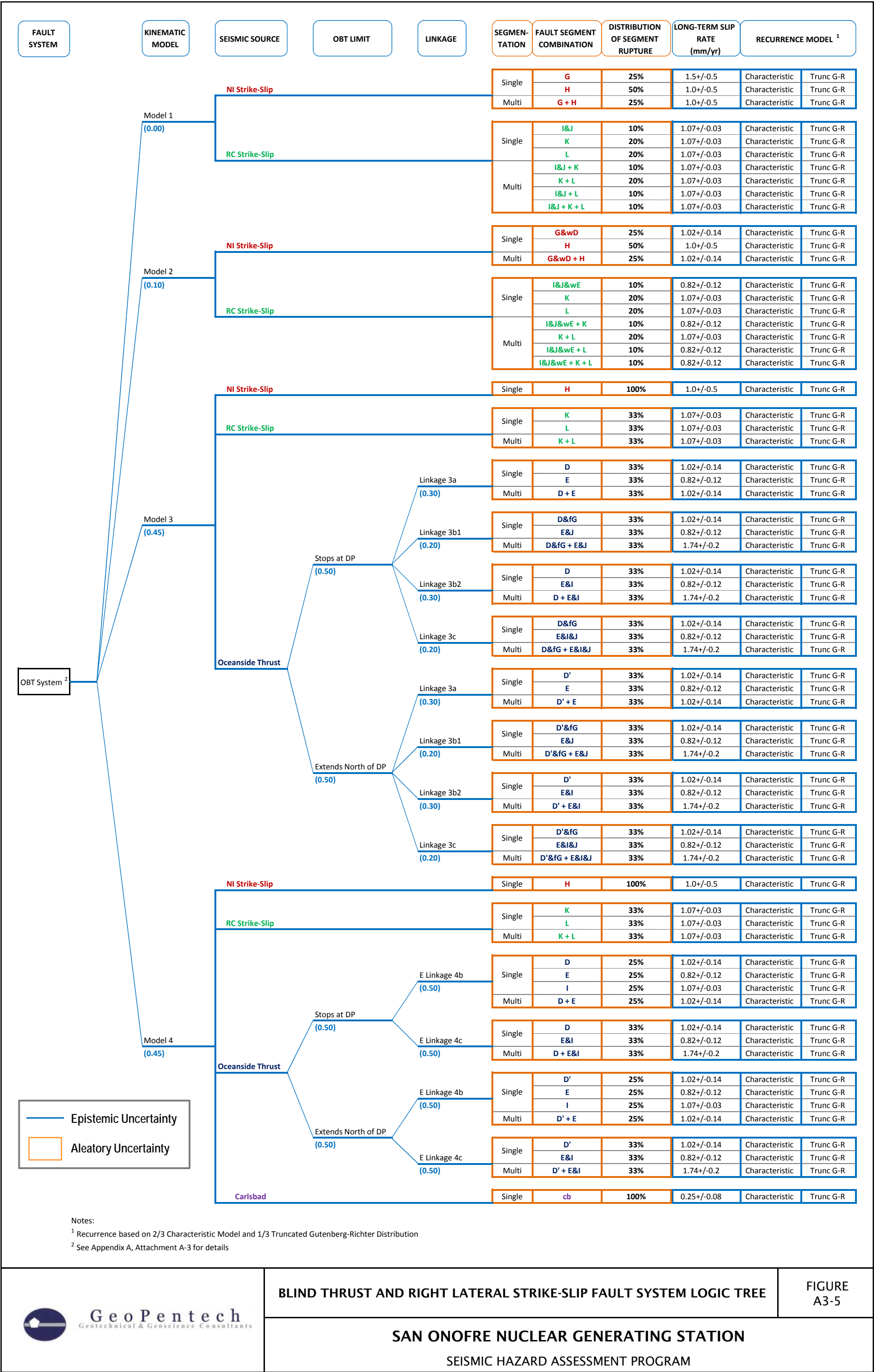
A3-4

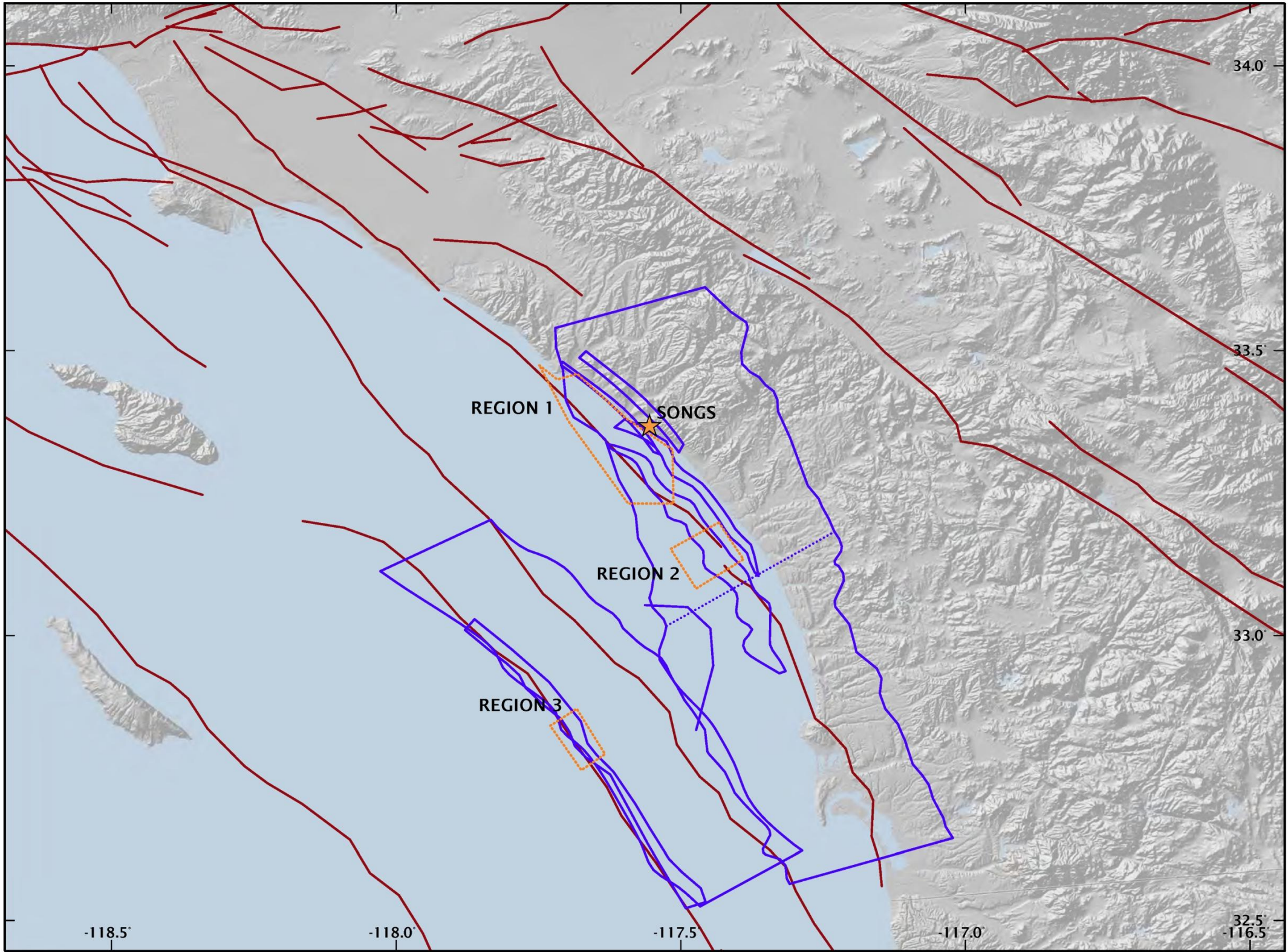
Notes:

¹Maximum Magnitude based on Wells & Coppersmith (1994)

²Value estimated by Rivero (2004) or Shaw & Plesch (2010)

³Recurrence Interval based on Shaw & Suppe (1996)





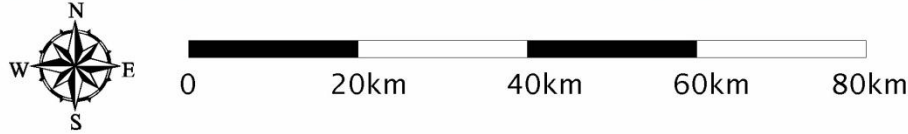
Legend

- ★ SONGS Facility Location
- Fault Systems from Rivero (2004)
- Fault Traces from USGS (2009)
- ▨ Areas Recommended for Future Study

| Region | Approx. Area |
|----------|---------------------|
| Region 1 | 250 km ² |
| Region 2 | 90 km ² |
| Region 3 | 50 km ² |

Notes:

Base map is shaded relief of southern California based on SRTM model prepared by ESRI, 2009.



APPENDIX B

2010 PSHA GROUND MOTION CHARACTERIZATION



APPENDIX B OUTLINE

- B1.0 INTRODUCTION**
- B2.0 QA/QC OF HAZ4.2 PSHA COMPUTER PROGRAM**
- B3.0 SHEAR WAVE VELOCITY PARAMETERS USED IN NGA RELATIONSHIPS**
- B4.0 GROUND MOTION PREDICTION EQUATION EPISTEMIC UNCERTAINTY**
- B5.0 RECURRENCE RELATIONSHIPS**



**APPENDIX B
2010 PSHA GROUND MOTION CHARACTERIZATION**

B1.0 INTRODUCTION

This Appendix provides further discussions on selected PSHA-related issues addressed in the main report. The selected issues consist of QA/QC work done on the PSHA computer program HAZ4.2 (Abrahamson, 2010); characterization of the site shear wave velocity parameters used in the attenuation relationships; epistemic uncertainty associated with the attenuation relationships used; and recurrence relationships for the hypothesized OBT source.

B2.0 QA/QC OF HAZ4.2 PSHA COMPUTER PROGRAM

The PSHA computer program HAZ4.2, developed by Dr. Norman Abrahamson (2010) as the newest version of his PSHA program, was selected for use in the 2010 PSHA. This latest version enabled SHAP to implement the NSHM 2009 (USGS, 2009, PC) seismic source model and adopt the UCERF 2 (WGCEP, 2008) time independent model for conducting PSHA. However, because HAZ4.2 had not yet gone through a QA/QC process, SHAP, guided by Dr. Norman Abrahamson, followed the PSHA Validation Project methodology described in Thomas et al. (2010) to initiate this QA/QC process. The process was completed for the elements of HAZ4.2 pertinent to this study, but not others. The resulting QA/QC'd portion of the HAZ4.2 computer program will be considered an interim version of HAZ4.2 on the 2010 PSHA. The actual process in completing the QA/QC'd portion of HAZ4.2 involved interactions of SHAP with Dr. Nicholas Gregor who works with Dr. Norman Abrahamson in developing the program. SHAP and Dr. Nicholas Gregor completed a series of computer runs followed by identifications and modification resolutions on various aspects of the computer program.

The purpose of the PSHA Validation Project (Thomas et al., 2010) was to develop a consistent method for testing several aspects of the PSHA calculation process for various, widely-used PSHA computer programs in the engineering community. The validation process consisted of test cases using strike-slip, reverse, and areal sources along with various site locations as illustrated on Figure B-1. Figure B-1 also shows the sites used in the validation. The test cases were designed to address calculation of site distance, rate, ground motion attenuation, hanging wall effects, earthquake recurrence, ground motion variability, and rupture area variability against hand-calculations whenever available. The test case results for each computer program were validated by comparing them to Pacific Earthquake Engineering Research (PEER) reported results by Thomas et al. (2010) for each test case.

SHAP compared the HAZ4.2 results for all test cases against the PEER reported results from Thomas et al. (2010). Figures B-2 and B-3 compare the HAZ4.2 results with the PEER reported results for two different cases as example results. As shown on Figures B-2 and B-3, the HAZ4.2 results match with the PEER reported results from Thomas et al. (2010). The comparisons of results shown on Figures B-2 and B-3 are representative of the remaining 104 cases considered. The final results for all test cases of the QA/QC process, when eventually completed, will be presented in a report titled "QA/QC of HAZ4.2 PSHA Computer Program."

B3.0 SHEAR WAVE VELOCITY PARAMETERS USED IN NGA RELATIONSHIPS



Table B-1 shows the attenuation relationships from the NGA models used in the PSHA. These attenuation relationships are called the NGA relationships herein and consist of the following:

- Abrahamson and Silva (2008)
- Boore and Atkinson (2008)
- Campbell and Bozorgnia (2008)
- Chiou and Youngs (2008)
- Idriss (2008)

Table B-1 also summarizes the estimated shear-wave velocity parameters for SONGS used in the NGA relationships, including 1) the average shear-wave velocity from the ground surface to a depth of 30 m (V_{s30}), 2) the approximate depth to 1 km/s shear-wave velocity material ($Z_{1.0}$), and 3) the approximate depth to 2.5 km/s shear-wave velocity material ($Z_{2.5}$). These shear wave velocity parameters, not all of them used by all five relationships listed above, were based on relevant data compiled from past reports documenting previous site investigations. Figures B-4 and B-5 present compilations of the site seismic velocity data from the ground surface to a depth of 30 m and 4,000 m, respectively. These figures show both shear- and pressure-wave data that was either directly measured in the site vicinity (colored solid lines) or was estimated based on other data (colored dashed lines). Also, a generalized stratigraphic column showing the geologic units is presented between the shear- and pressure-wave graphs on Figures B-4 and B-5. This geologic interpretation is based on data presented in Dames & Moore (1970) and SCE (2001).

As shown on Figures B-4 and B-5, the pressure-wave velocities at the site were directly measured from 1) a surface seismic velocity survey by Dames & Moore (1970), 2) an acoustic velocity survey of borehole B-1 by Dames & Moore (1970), 3) a downhole seismic velocity survey by Weston Geophysical (1971), 4) an offshore seismic reflection survey by Western Geophysical (1972), and 5) geophysical data compiled by Dames & Moore (1970) to the base of the San Onofre Breccia (Tso) or to a depth of approximately 1,525 m (5,000 ft). Below the base of the San Onofre Breccia, the pressure-wave data was estimated by Dames & Moore (1970) based on measurements performed within the deeper rock units in the region by others.

As shown on Figures B-4 and B-5, the shear-wave velocities at the site were directly measured from 1) a surface seismic velocity survey by Dames & Moore (1970), 2) a downhole seismic velocity survey by Weston Geophysical (1971), 3) Rayleigh wave tests by Woodward-McNeill (1974), and 4) geophysical data compiled by Dames & Moore (1970) to the base of the Monterey Formation Tm (see Figure B-5) or to a depth of approximately 760 m (2,500 ft).

Shear-wave velocities at the site were also estimated based on pressure-wave velocities, Poisson's ratio, and shear modulus relationships. As shown on Figures B-4 and B-5, shear-wave velocities below the base of the Monterey Formation were computed by Dames & Moore (1970) from pressure-wave velocities and estimates of the Poisson's ratio measured in similar materials. Estimates of the shear-wave velocity were also calculated from the acoustic velocity log within B1 shown on Figures B-4 and B-5 (Dames & Moore, 1970) and the offshore seismic pressure-wave data (Western Geophysical, 1972) using the

Poisson's ratio values presented in Dames & Moore (1970). Lastly, shear-wave velocities estimates were calculated based on shear modulus relationships presented in Woodward-McNeill (1972). These estimates were calculated for the San Mateo Formation to a depth of 285 m (935 ft).

The San Mateo Formation sandstone comprises the first 30 m of geologic material beneath SONGS. As shown on Figure B-4, the shear-wave velocities measured or estimated within the first 30 m below the site are relatively similar to each other with the widest spread in values in the near-surface between approximately 0 and 12 m. The V_{s30} values based on Dames & Moore (1970) data (solid yellow and red lines on Figure B-4) and estimated based on offshore data by Western Geophysical (1972) (dashed green line on Figure B-4) are approximately 670 m/s and 730 m/s, respectively. These V_{s30} values were based on widely spaced survey data and pressure-wave velocity measurements that resulted in poor resolution of the near-surface shear-wave velocity values. Investigations resulting in a higher resolution of near-surface shear-wave velocities were performed by Weston (1971) (solid magenta line on Figure B-4) and Woodward-McNeill (1974) (solid purple line on Figure B-4). The V_{s30} based on the Weston (1971) data is approximately 500 m/s. The V_{s30} value was also calculated by combining the Woodward-McNeill (1974) data (solid purple line), which had a maximum exploration depth of about 4.5 m, with the shear-wave velocity estimated based on the San Mateo Formation's shear modulus relationship developed by Woodward-McNeill (1972) (dashed cyan line on Figure B-4). As shown on Figure B-4, this combined V_{s30} is about 500 m/s, which is the same as the V_{s30} based on the Weston (1971) data. Since the Weston and Woodward-McNeill data provided the best resolution of shear-wave velocities within the first 30 m of the San Mateo Formation, the V_{s30} within the San Mateo Formation at the site is estimated to be 500 m/s for the NGA relationships in Table B-1.

As shown on Figure B-5, the estimated $Z_{1.0}$ varies depending on the source of the shear-wave velocity data. The upper bound of $Z_{1.0}$ is approximately 135 m and is based on the San Mateo Formation shear modulus relationship developed by Woodward-McNeill (1972) (dashed cyan line on Figure B-5). The $Z_{1.0}$ based on the Dames and Moore (1970) data (solid red line on Figure B-5) and Western Geophysical (1972) data (dashed green line on Figure B-5) is approximately 610 m and 305 m, respectively. This puts the $Z_{1.0}$ at the top of the Monterey Formation, which varies between the two sources. It is noted that the top of the Monterey Formation at the site, as shown on the geology log on Figure B-5, is based on the Western Geophysical (1972) offshore seismic data presented in SCE (2001), and includes the latest geologic interpretation. This latest geologic interpretation together with the idea that the $Z_{1.0}$ depth occurs at the top of the Monterey Formation leads to a $Z_{1.0}$ depth of approximately 305 m, which was used in the NGA relationships in Table B-1. This value is similar to the average of all $Z_{1.0}$ sources, which is approximately 350 m.

Dames and Moore (1970) provides the only site-specific shear-wave data below the base of the Monterey Formation (dashed red lines on Figure B-5). As shown on Figure B-5, the $Z_{2.5}$ is estimated to occur at approximately 3,350 m, which corresponds to the approximate top of the crystalline basement igneous and metamorphic rocks.

B4.0 GROUND MOTION PREDICTION EQUATION EPISTEMIC UNCERTAINTY

The attenuation relationships associated with the NGA work are often referred to as the GMPE. In using attenuation relationships, their epistemic uncertainty should be considered. In the past, this epistemic

uncertainty was often accommodated by using multiple attenuation relationships. However, given the coordinated process used to develop the NGA relationships, it should not be adequate to address this epistemic uncertainty by just using multiple NGA relationships. An epistemic GMPE uncertainty in addition to the use of five NGA relationships was reflected in the PSHA herein as described below.

The additional epistemic uncertainty follows USGS (2008) as summarized below:

The USGS applies the epistemic uncertainty d_{gnd} symmetrically (USGS, 2008) so that the weights for $(\ln(gnd)+d_{gnd})$ and $(\ln(gnd)-d_{gnd})$ are the same at 0.185 and the unmodified $\ln(gnd)$ has a weight of 0.63. Here, $\ln(gnd)$ stands for the natural logarithm of the median peak or spectral acceleration, “gnd”, for a given attenuation relationship. The term “ d_{gnd} ” stands for the median or spectral acceleration uncertainty for any given attenuation relationship.

Due to the limitations of the data (particularly for large earthquakes) used in developing the NGA relationships and the considerable interactions that took place among the NGA modelers (USGS, 2008), NGA modelers suggested that the NGA relationships should also incorporate epistemic uncertainty (beyond using multiple relationships). Following the NGA modelers' suggestion, the USGS partitioned the source space into nine (9) bins determined by three partitions in the distance space (0 to 10 km, 10 to 30 km, and larger than 30 km) and three partitions in the magnitude space (5 to 6, 6 to 7, and larger than 7) as shown in Table B-2. However, of all the attenuation relationships considered by the USGS, only Campbell and Bozorgnia (2008) and Chiou and Youngs (2008) provided sufficient information to estimate the epistemic uncertainty within the nine bins considered. Based on an average epistemic uncertainty, Table B-2 shows the resulting epistemic uncertainty within each of the 9 bins considered by the USGS (2008).

As in the USGS evaluation, the space was divided into 9 bins (3 ranges in the magnitude space and 3 ranges in the distance space). Within each bin, an average value of the range was used to compute the peak or spectral accelerations for all 5 attenuation relationships considered. For example, in the case of the magnitude range 6 to 7, and distance the range 0 to 10 km, an average magnitude value of 6.5 and an average rupture distance of 5 km was used to compute the spectral ordinates from all 5 attenuation relationships. Figures B-6 and B-7 show the computed spectral ordinates for strike-slip and reverse faulting mechanism, respectively. Next, the ratio of the maximum to minimum calculated spectral accelerations was computed for each frequency. Figure B-8 shows the resulting ratios for each of the two styles of faulting mechanism considered, as well as their average values within the range of frequencies of interest. In general, the average ratio for the reverse faulting mechanism tends to be larger than that of the strike-slip faulting mechanism. In the present evaluation, average ratios obtained from the reverse faulting mechanism were used.

The epistemic uncertainty from the attenuation relationships can be compared to the epistemic uncertainty values provided by the USGS by noting that the minimum and maximum spectral accelerations are provided by $(\ln(gnd)-d_{gnd})$ and $(\ln(gnd)+d_{gnd})$, respectively. Therefore, in the USGS case, the ratio of maximum (“max”) to minimum (“min”) response spectra is provided by:

$$Sa_{Max,USGS}/Sa_{Min,USGS} = \exp[\ln(gnd) + d_{gnd}] / \exp[\ln(gnd) - d_{gnd}]$$

$$Sa_{Max,USGS}/Sa_{Min,USGS} = \exp(2 \times d_{gnd})$$

where $Sa_{Max,USGS}/Sa_{Min,USGS}$ is the ratio of the maximum and minimum USGS spectral acceleration. Conversely, for a given average ratio value, the corresponding epistemic $dgnd$ term can also be computed as follows:

$$dgnd = \ln(Sa_{Max,USGS}/Sa_{Min,USGS})/2$$

In the example case cited above, the comparison of the USGS epistemic uncertainty ratio and the attenuation relationship epistemic uncertainty is shown on Figure B-9. The computed $dgnd$ term obtained from the attenuation relationship epistemic uncertainty is provided in Table B-3.

A comparison of the $dgnd$ terms provided by the USGS listed in Table B-2 and the attenuation relationship epistemic uncertainty listed in Table B-3 is also shown in graphical form on Figure B-10.

The results from the use of the five attenuation relationships already reflect some epistemic uncertainty from the attenuation relationships. In order to account for the “full” GMPE epistemic uncertainty due to the lack of data, the difference between the two $dgnd$ values for each of the nine bins above needs to be considered. The final epistemic uncertainty included in the current study is provided in Table B-4.

In this study, the events controlling the shaking condition at the site were mainly magnitude 6 to 7 events with a distance range of less than 10 km. Therefore, the epistemic uncertainty for this magnitude range and distance range is the only one that was used for all five attenuation relationships considered in the PSHA evaluation.

B5.0 RECURRENCE RELATIONSHIPS

The recurrence relationships used for the NI/RC Fault Zone source were based on the time-independent part of the UCERF 2 and followed the UCERF 2 methodology (WGCEP, 2008). Following this methodology, a characteristic recurrence relationship (Youngs and Coppersmith, 1985) was assigned a weight of 2/3, and a truncated exponential relationship (Youngs and Coppersmith, 1985) was assigned a weight of 1/3. For the hypothesized OBT source, which was not based on the UCERF 2, appropriate recurrence relationships to be used were guided in part by available historic seismicity data.

Figure B-11 shows 1) the limited observed historic main shock seismicity evaluated for completeness in the area of SONGS and 2) a region generally within 10 km of the hypothesized OBT used in the evaluation of historic seismicity data for the hypothesized OBT source. The historic seismicity catalog and general methodologies used to process this catalog are from UCERF2 (WGCEP, 2008). Figure B-12 shows the hypothesized OBT earthquake recurrence based on the observed historic earthquakes within the hypothesized OBT region (five total, as shown on Figure B-11). The historic seismicity model shown on Figure B-12 includes: 1) the cumulative annual frequency of occurrence of various magnitude or greater observed earthquakes (shown as open circles) and 2) the upper and lower standard deviation recurrence bounds based on Weichert (1980) (shown as vertical bars). Figure B-12 also shows the earthquake recurrence relationship developed using the seismic source parameters for the hypothesized OBT source (Section 2.0 and Appendix B) and assuming only the characteristic recurrence model by Youngs and Coppersmith (1985). As shown on Figure B-12, the use of only the characteristic recurrence relationship to represent the hypothesized OBT source results in the recurrence relationship that is reasonably consistent with the historic seismicity in the hypothesized OBT region. On the basis of

**SAN ONOFRE NUCLEAR GENERATING STATION
SEISMIC HAZARD ASSESSMENT PROGRAM
2010 PROBABILISTIC SEISMIC HAZARD ANALYSIS REPORT**

the results shown on Figure B-12, only the characteristic recurrence relationship was used to represent the hypothesized OBT source.



TABLE B-1
NGA Relationships and Shear-wave Velocity Parameters

| NGA | Epistemic Weight | Shear-Wave Velocity Parameters† | | |
|-------------------------------|------------------|---------------------------------|--------------|---------------|
| | | V_{s30} * | $Z_{1.0}$ ** | $Z_{2.5}$ *** |
| Abrahamson and Silva (2008) | 0.20 | 500-m/s | 0.31-km | 3.35-km |
| Boore and Atkinson (2008) | 0.20 | | | |
| Campbell and Bozorgnia (2008) | 0.20 | | | |
| Chiou and Youngs (2008) | 0.20 | | | |
| Idriss (2008) | 0.20 | | | |

†Used as needed in each NGA relationship

* V_{s30} = the average shear wave velocity from the ground surface to a depth of 30-m

** $Z_{1.0}$ = the approximate depth to 1.0 km/s shear wave velocity material

*** $Z_{2.5}$ = the approximate depth to 2.5 km/s shear wave velocity material

TABLE B-2
Epistemic Uncertainty in the GMPE (natural log term)

| Magnitude Range | Rupture Distance Range | Average <i>dgnd</i> Term |
|-----------------|------------------------|--------------------------|
| 5 to 6 | 0 to 10km | ± 0.375 |
| | 10 to 30km | 0.21 |
| | ≥ 30 km | 0.245 |
| 6 to 7 | 0 to 10km | 0.23 |
| | 10 to 30km | 0.225 |
| | ≥ 30 km | 0.23 |
| ≥ 7 | 0 to 10km | 0.40 |
| | 10 to 30km | 0.36 |
| | ≥ 30 km | 0.31 |

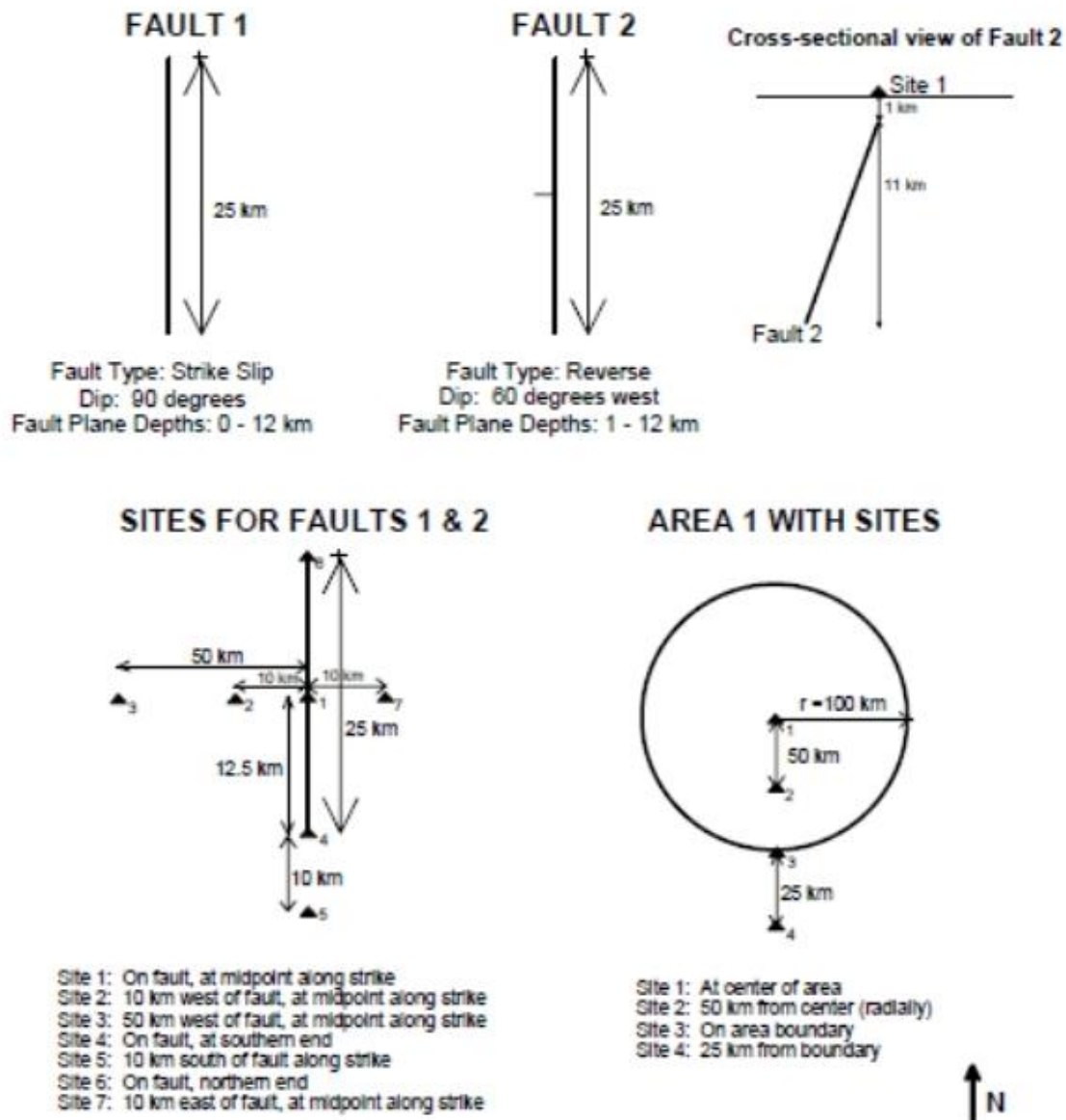
TABLE B-3
Epistemic Uncertainty in the Attenuation Relationships (natural log term)

| Magnitude Range | Rupture Distance Range | Average <i>dgnd</i> Term |
|-----------------|------------------------|--------------------------|
| 5 to 6 | 0 to 10km | ± 0.285 |
| | 10 to 30km | 0.252 |
| | ≥ 30 km | 0.293 |
| 6 to 7 | 0 to 10km | 0.157 |
| | 10 to 30km | 0.15 |
| | ≥ 30 km | 0.208 |
| ≥ 7 | 0 to 10km | 0.17 |
| | 10 to 30km | 0.154 |
| | ≥ 30 km | 0.147 |

TABLE B-4
Epistemic Uncertainty (natural log term) Used in the Current Study

| Magnitude Range | Rupture Distance Range | Average <i>dgnd</i> Term |
|-----------------|------------------------|--------------------------|
| 5 to 6 | 0 to 10km | ± 0.090 |
| | 10 to 30km | 0.0* |
| | ≥ 30 km | 0.0* |
| 6 to 7 | 0 to 10km | 0.073 |
| | 10 to 30km | 0.075 |
| | ≥ 30 km | 0.022 |
| ≥ 7 | 0 to 10km | 0.230 |
| | 10 to 30km | 0.206 |
| | ≥ 30 km | 0.163 |

* signifies that when the *dgnd* value from the attenuation relationships exceeds the USGS *dgnd* value, an epistemic uncertainty value of 0.0 was conservatively used.

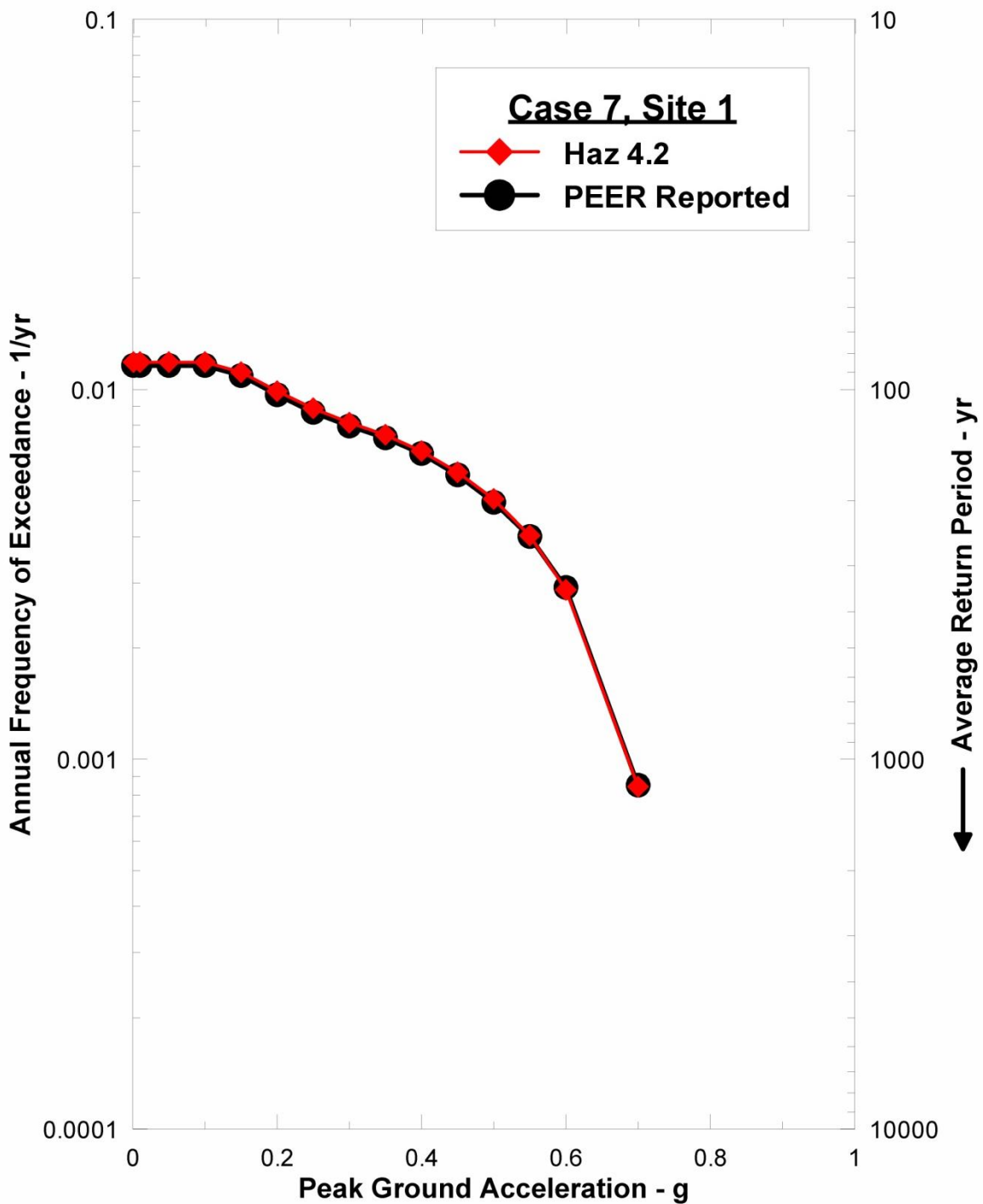


GeoPentech
Geotechnical & Geoscience Consultants

QA/QC OF HAZ4.2 –
FAULT AND SITE GEOMETRY FOR TEST CASES

FIGURE
B-1

SAN ONOFRE NUCLEAR GENERATING STATION
SEISMIC HAZARD ASSESSMENT PROGRAM

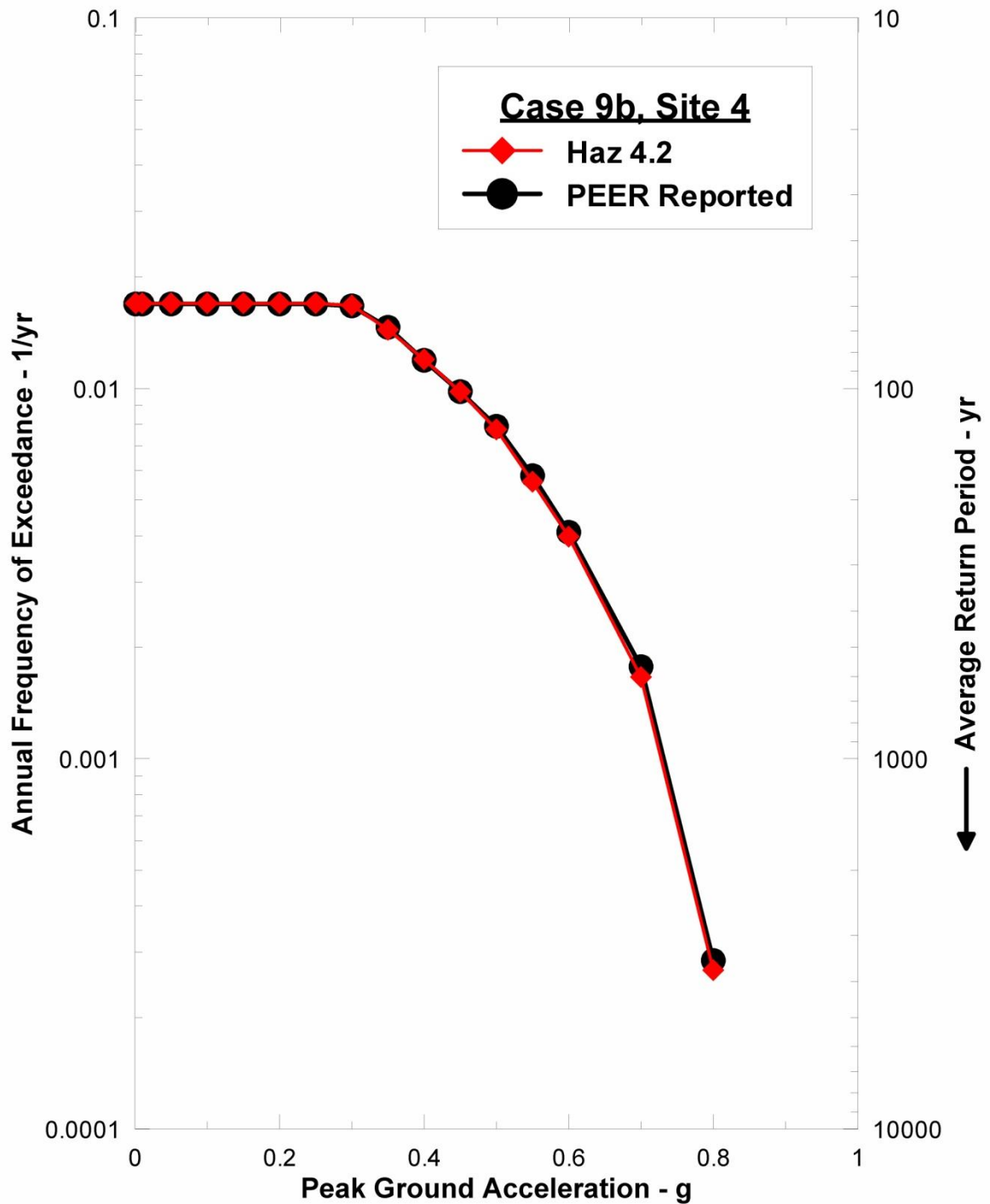


GeoPentech
Geotechnical & Geoscience Consultants

QA/QC OF HAZ4.2 -
TEST CASE 7, SITE 1

FIGURE
B-2

SAN ONOFRE NUCLEAR GENERATING STATION
SEISMIC HAZARD ASSESSMENT PROGRAM

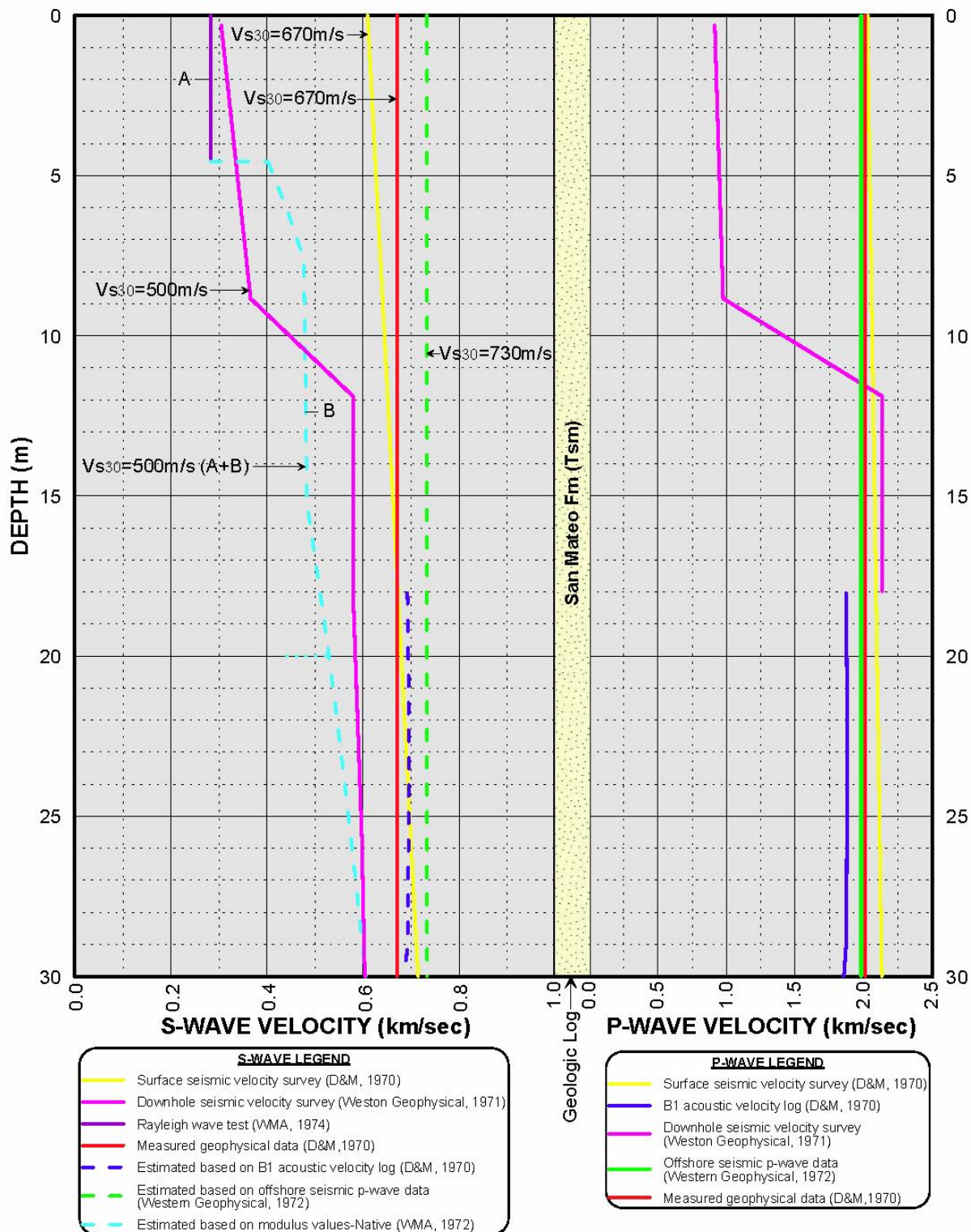


GeoPentech
Geotechnical & Geoscience Consultants

QA/QC OF HAZ4.2 -
TEST CASE 9b, SITE 4

FIGURE
B-3

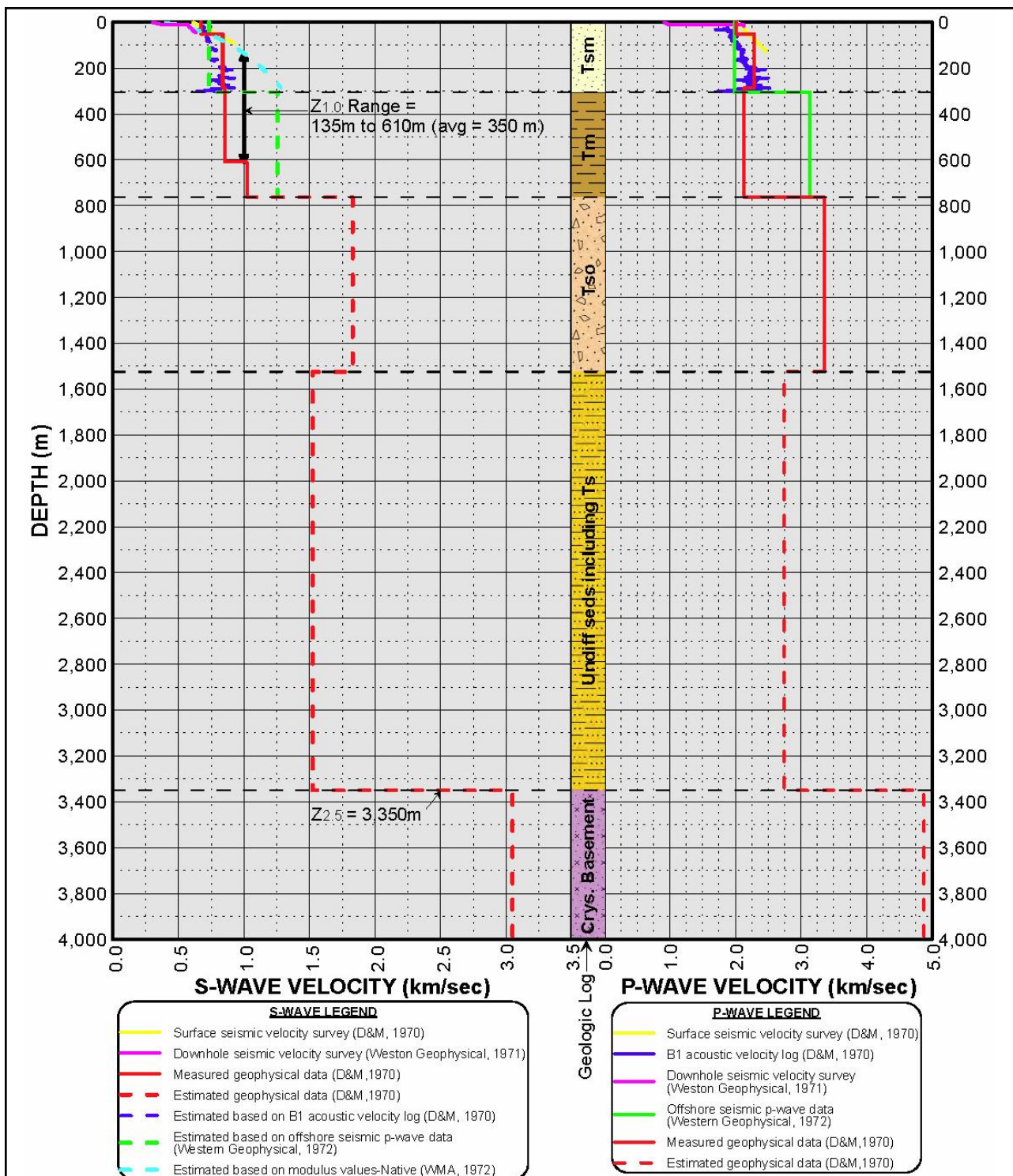
SAN ONOFRE NUCLEAR GENERATING STATION
SEISMIC HAZARD ASSESSMENT PROGRAM



SHEAR- WAVE AND PRESSURE- WAVE VELOCITY SUMMARY (0 to 30 m)

**FIGURE
B-4**

SAN ONOFRE NUCLEAR GENERATING STATION SEISMIC HAZARD ASSESSMENT PROGRAM



NOTE: Geology based on D&M (1970) and SCE (2001).

Tsm= San Mateo Fm.; Tso=San Onofre Breccia; Ts=Santiago Fm.

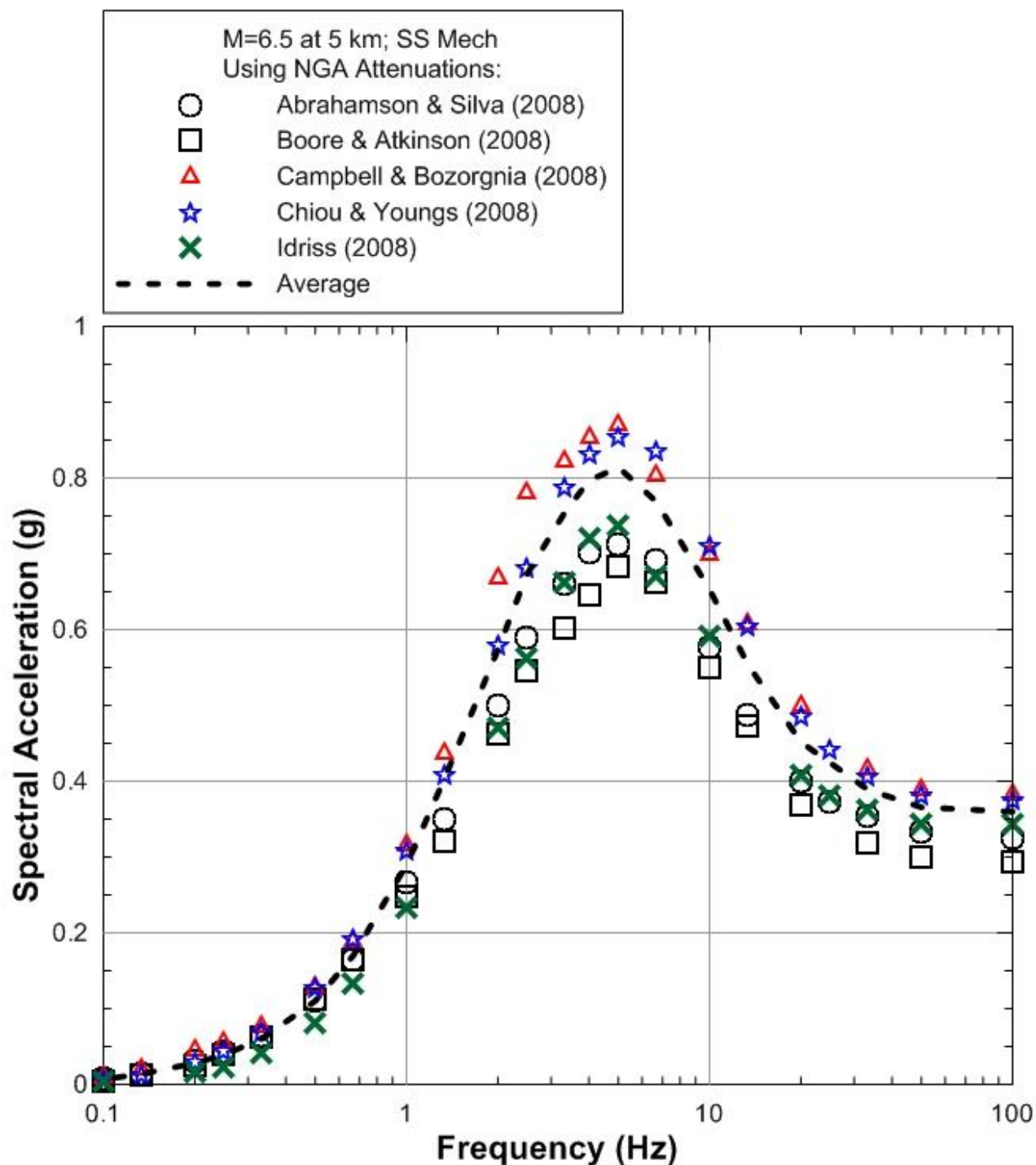


GeoPentech
Geotechnical & Geoscience Consultants

SHEAR- WAVE AND PRESSURE- WAVE VELOCITY SUMMARY (0 to 4,000 m)

FIGURE
B-5

SAN ONOFRE NUCLEAR GENERATING STATION SEISMIC HAZARD ASSESSMENT PROGRAM



NOTE: Mw=6.5 at 5 km for strike-slip faulting mechanism

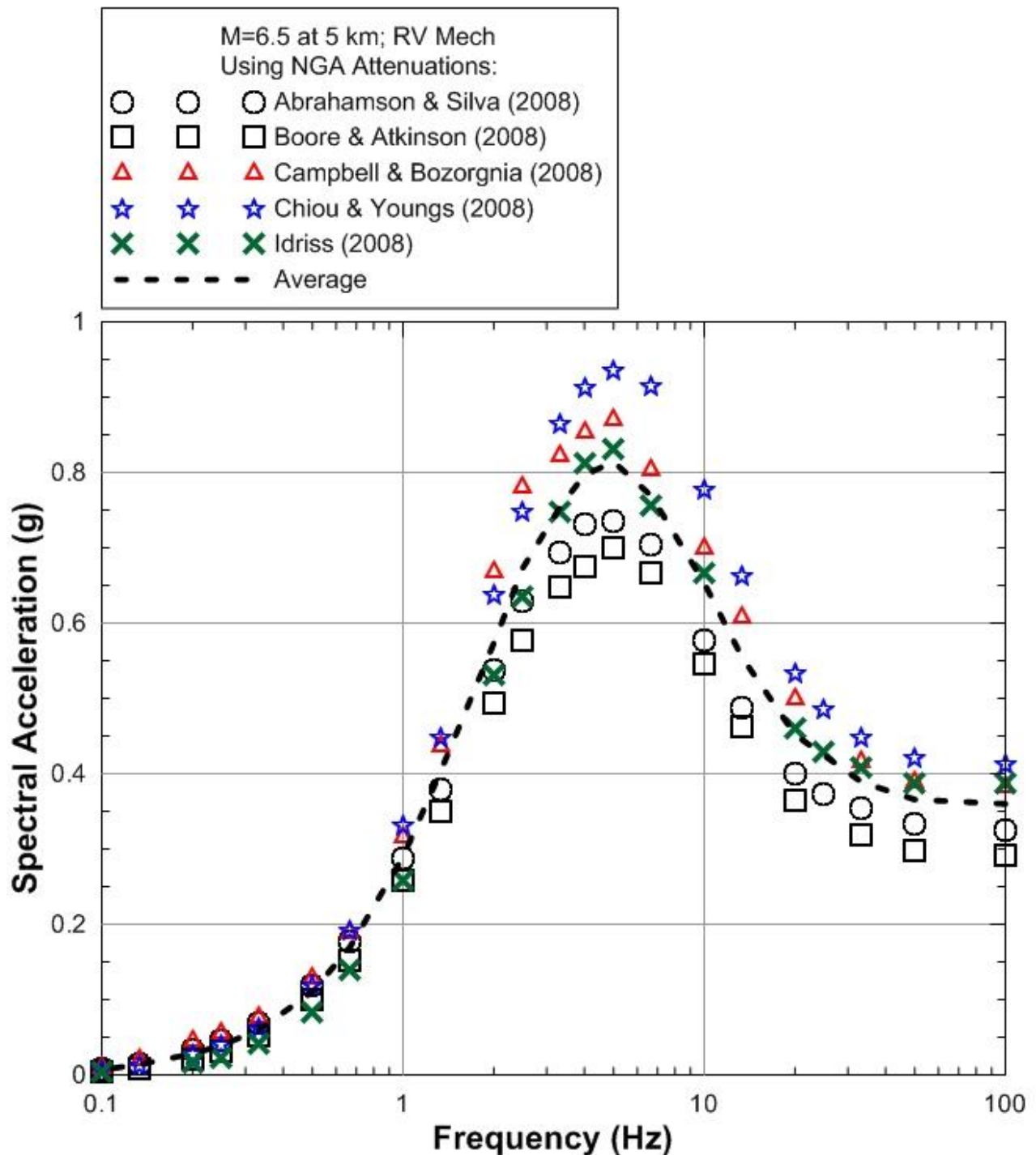


GeoPentech
Geotechnical & Geoscience Consultants

**RESPONSE SPECTRA FOR THE 5 NGA
ATTENUATION RELATIONSHIPS USED**

**FIGURE
B-6**

SAN ONOFRE NUCLEAR GENERATING STATION
SEISMIC HAZARD ASSESSMENT PROGRAM



NOTE: Mw=6.5 at 5 km for reverse faulting mechanism

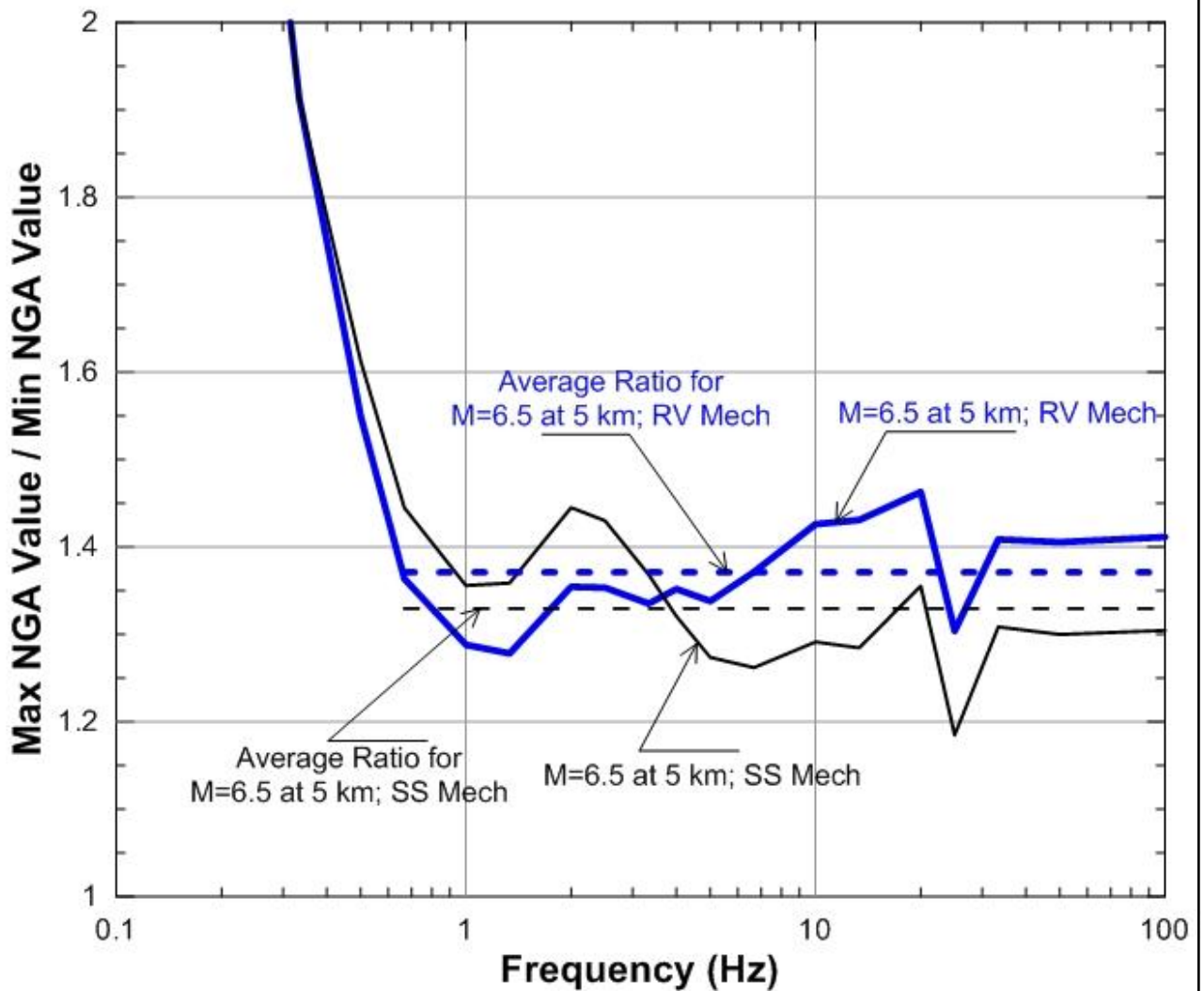


GeoPentech
Geotechnical & Geoscience Consultants

RESPONSE SPECTRA FOR THE 5 NGA
ATTENUATION RELATIONSHIPS USED

FIGURE
B-7

SAN ONOFRE NUCLEAR GENERATING STATION
SEISMIC HAZARD ASSESSMENT PROGRAM



NOTE: Mw=6.5 at 5 km for strike-slip and reverse faulting mechanism

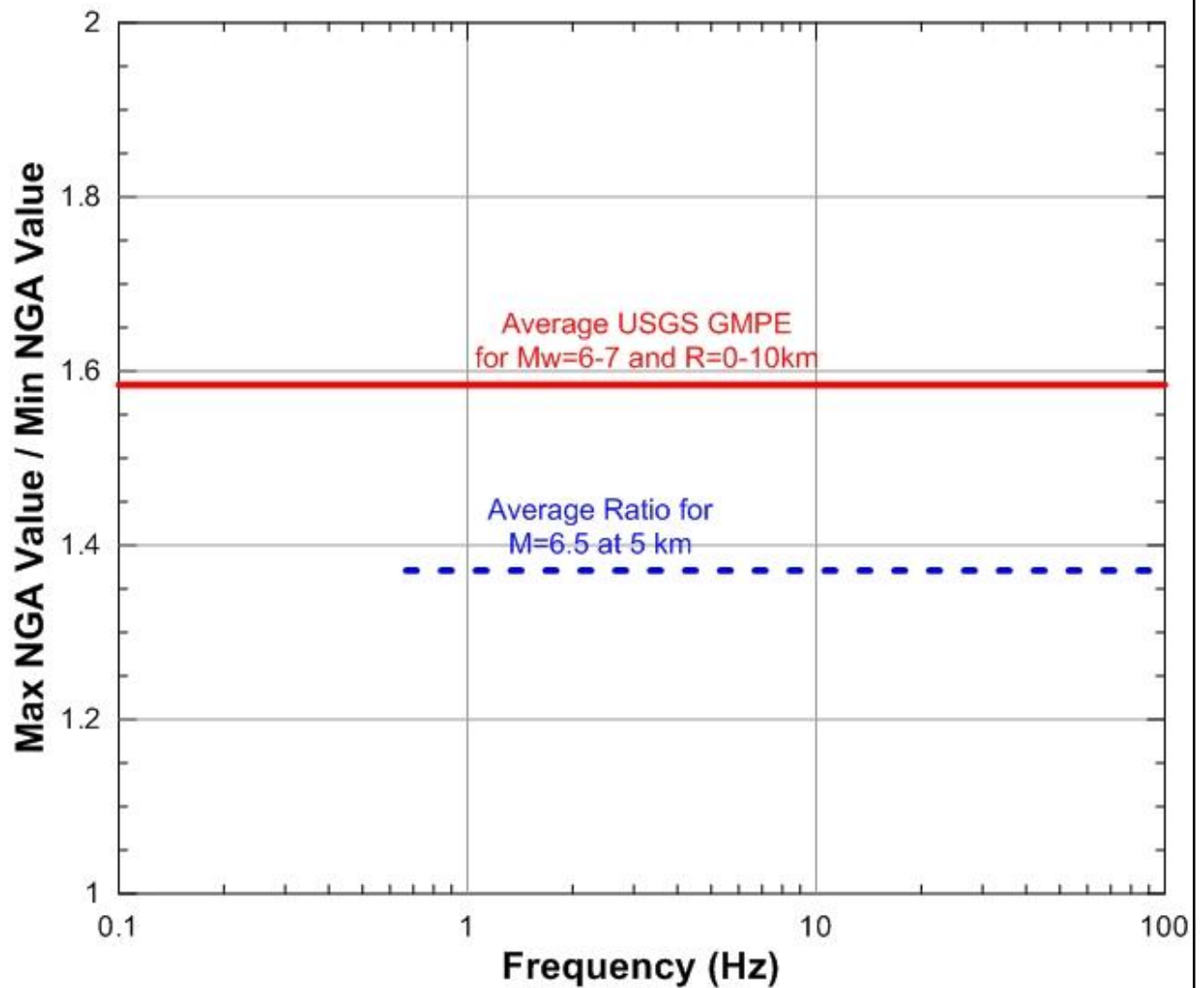


GeoPentech
Geotechnical & Geoscience Consultants

**RATIOS OF MAXIMUM TO MINIMUM
SPECTRAL ACCELERATIONS**

**FIGURE
B-8**

SAN ONOFRE NUCLEAR GENERATING STATION
SEISMIC HAZARD ASSESSMENT PROGRAM



NOTE: Mw=6-7, R=0-10 km

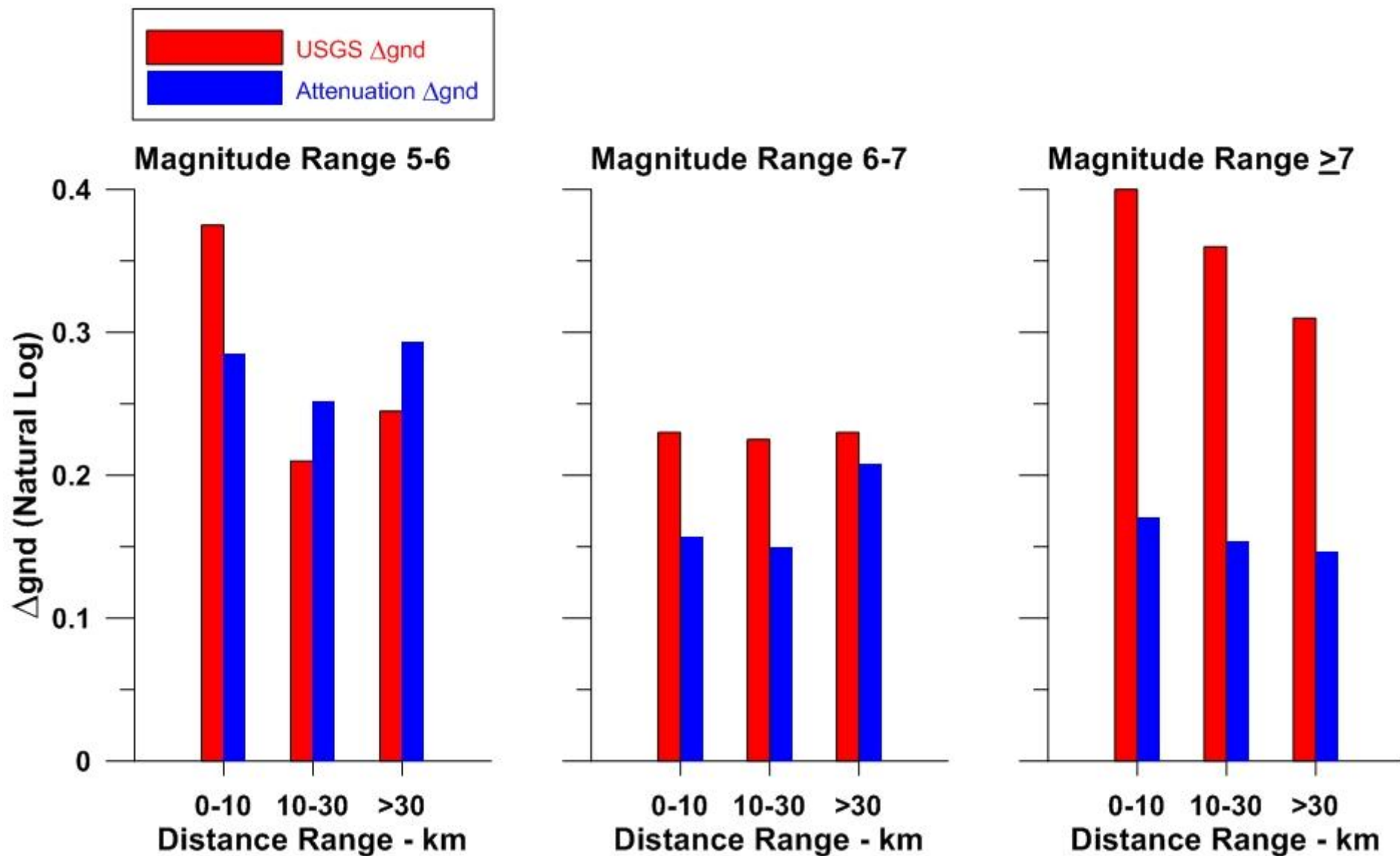


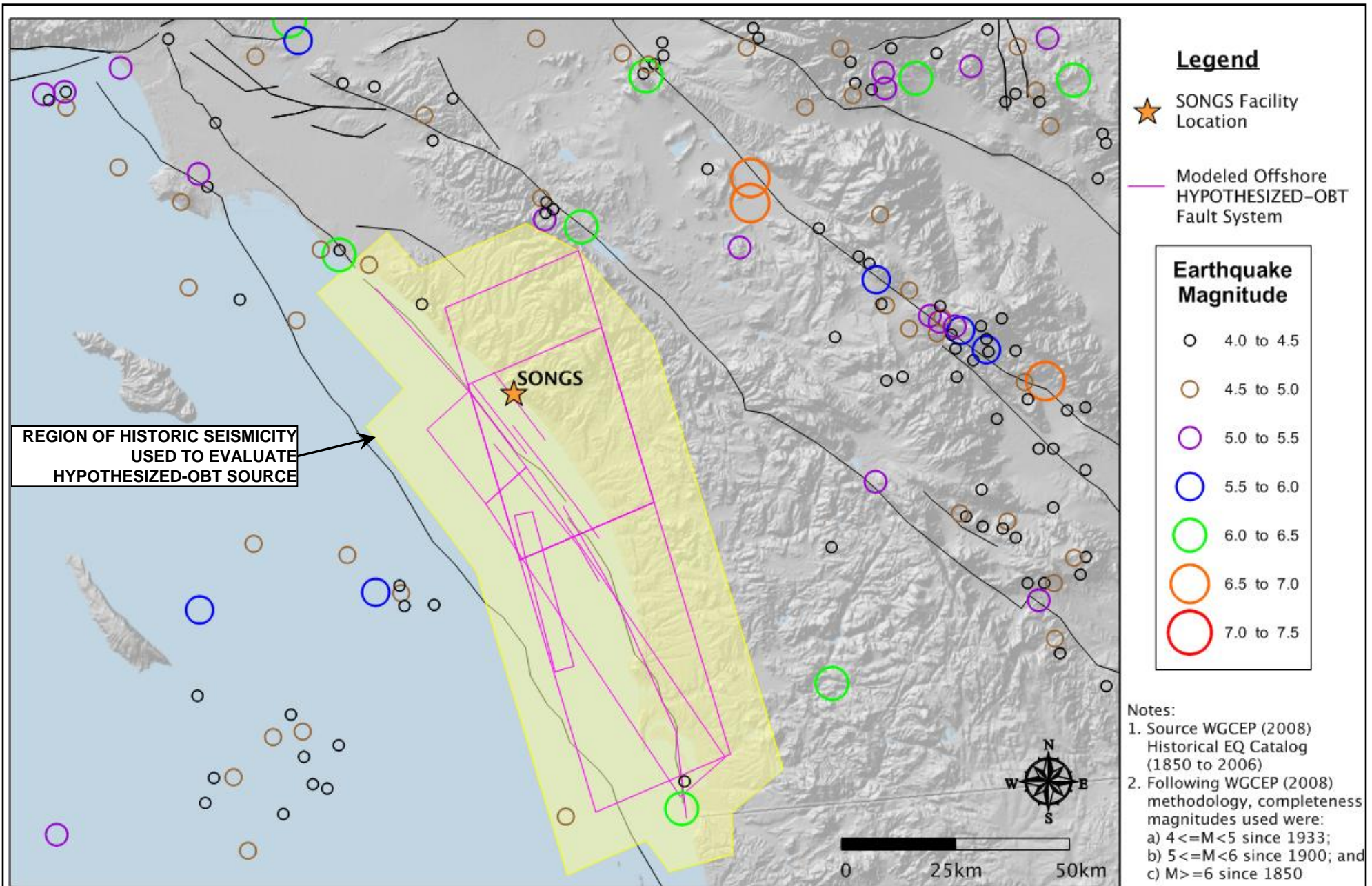
GeoPentech
Geotechnical & Geoscience Consultants

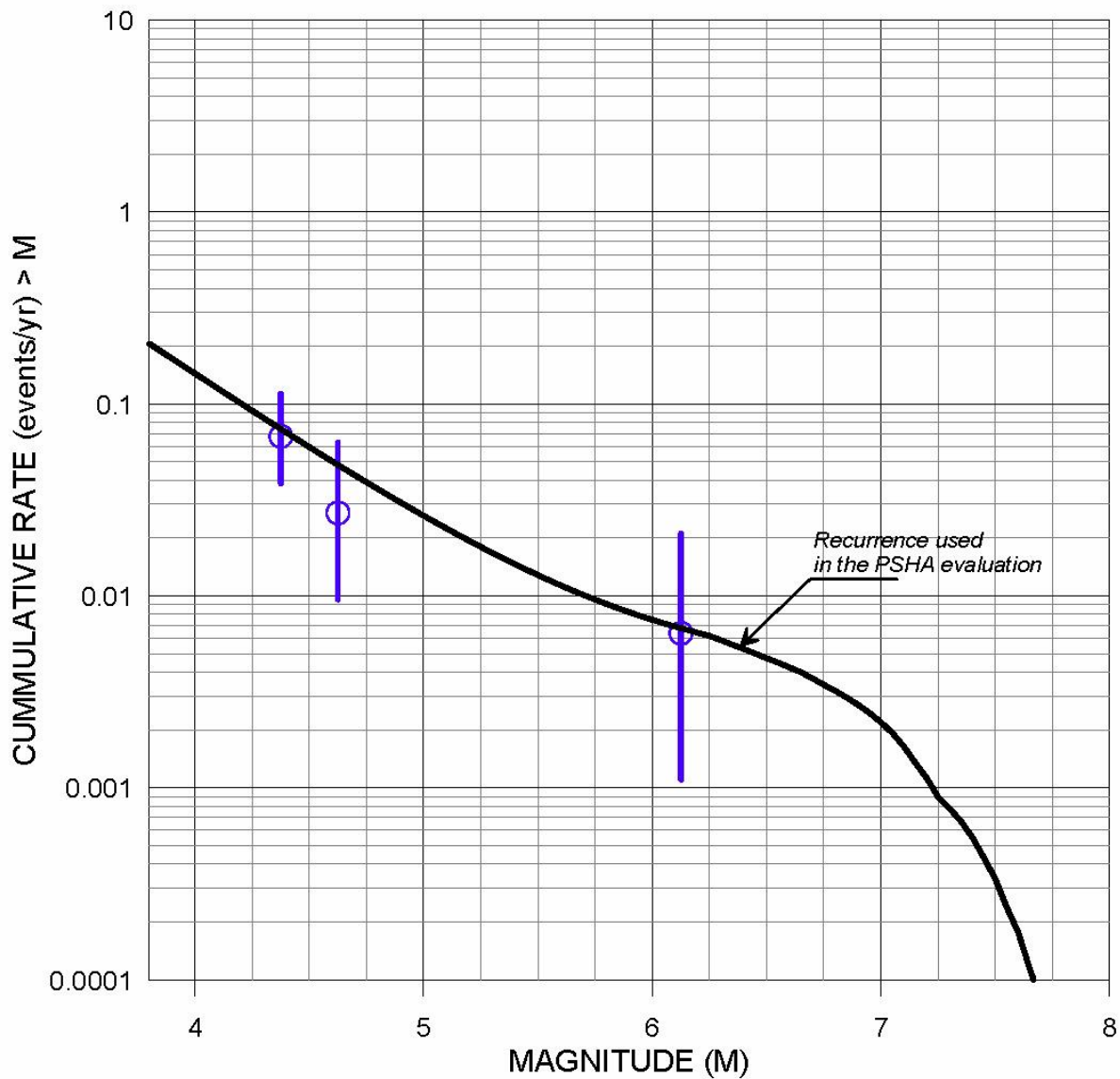
COMPARISON OF USGS EPISTEMIC UNCERTAINTY AND
ATTENUATION RELATIONSHIP EPISTEMIC UNCERTAINTY

FIGURE
B-9

SAN ONOFRE NUCLEAR GENERATING STATION
SEISMIC HAZARD ASSESSMENT PROGRAM







GeoPentech
Geotechnical & Geoscience Consultants

**COMPARISON OF HISTORICAL
AND MODEL RECURRENCES**

**FIGURE
B-12**

SAN ONOFRE NUCLEAR GENERATING STATION
SEISMIC HAZARD ASSESSMENT PROGRAM